SIAM J. Imaging Sciences
Vol. 6, No. 3, pp. 1499–1530

Estimation Method of the Homodyned K-Distribution Based on the Mean Intensity and Two Log-Moments*

François Destrempes†, Jonathan Porée‡, and Guy Cloutier§

Abstract. The homodyned K-distribution appears naturally in the context of random walks and provides a useful model for the distribution of the received intensity in a wide range of non-Gaussian scattering configurations, including medical ultrasonics. An estimation method for the homodyned K-distribution based on the first moment of the intensity and two log-moments (XU method), namely the X- and U-statistics previously studied in the special case of the K-distribution, is proposed as an alternative to a method based on the first three moments of the intensity (MI method) or the amplitude (MA method), and a method based on the signal-to-noise ratio (SNR), the skewness, and the kurtosis of two fractional orders of the amplitude (labeled RSK method). Properties of the X- and U-statistics for the homodyned K-distribution are proved, except for one conjecture. Using these properties, an algorithm based on the bisection method for monotonous functions was developed. The algorithm has a geometric rate of convergence. Various tests were performed to study the behavior of the estimators. It was shown with simulated data samples that the estimations of the parameters $1/\alpha$ and $1/(\kappa+1)$ of the homodyned K-distribution are preferable to the direct estimations of the clustering parameter α and the structure parameter κ (with respective relative root mean squared errors (RMSEs) of 0.63 and 0.13, as opposed to 1.04 and 4.37, when $N = 1000$). Tests on simulated ultrasound images with only diffuse scatterers (up to 10 per resolution cell) indicated that the XU estimator is overall more reliable than the other three estimators for the estimation of $1/\alpha$, with relative RMSEs of 0.79 (MI), 0.61 (MA), 0.53 (XU), and 0.67 (RSK). For the parameter $1/(\kappa+1)$, the relative RMSEs were equal to 0.074 (MI), 0.075 (MA), 0.069 (XU), and 0.100 (RSK). In the case of a large number of scatterers (11 to 20 per resolution cell), the relative RMSEs of $1/\alpha$ were equal to 1.43 (MI), 1.27 (MA), 1.25 (XU), and 1.33 (RSK), and the relative RMSEs of $1/(\kappa+1)$ were equal to 0.14 (MI), 0.16 (MA), 0.17 (XU), and 0.20 (RSK). The four methods were also tested on simulated ultrasound images with a variable density of periodic scatterers to test images with a coherent component. The addition of noise on ultrasound images was also studied. Results showed that the XU estimator was better overall than the other three. Finally, on the simulated ultrasound images, the average computation times per image were equal to 6.0 ms (MI), 8.0 ms (MA), 6.8 ms (XU), and 500 ms (RSK). Thus, a fast, reliable, and novel algorithm for the estimation of the homodyned K-distribution was proposed.

Key words. homodyned K-distribution, statistical parameter estimation, random walks, non-Gaussian scattering, optical propagation through turbulent media, microwave sea echo, land clutter, medical ultrasonics, echo envelope.

---

*Received by the editors May 2, 2012; accepted for publication (in revised form) April 9, 2013; published electronically August 1, 2013. This research was jointly supported by the Collaborative Health Research Program of the Natural Sciences and Engineering Research Council of Canada (NSERC, 365656-09) and Canadian Institutes of Health Research (CPG-95288), and by the Discovery grant program of NSERC (138570-11).

http://www.siam.org/journals/siims/6-3/87572.html

†Laboratory of Biorheology and Medical Ultrasonics, University of Montreal Hospital Research Center (CRCHUM), Montréal H2L-2W5, QC, Canada (francois.destrempes@crchum.qc.ca).

‡Laboratory of Biorheology and Medical Ultrasonics, University of Montreal Hospital Research Center (CRCHUM), Montréal H2L-2W5, QC, Canada, and Institute of Biomedical Engineering, University of Montreal, Montréal H3T-1J4, QC, Canada (jonathan.poree@gmail.com).

§Laboratory of Biorheology and Medical Ultrasonics, University of Montreal Hospital Research Center (CRCHUM), Montréal H2L-2W5, QC, Canada; Department of Radiology, Radio-Oncology and Nuclear Medicine, University of Montreal, Montréal H3T-1J4, QC, Canada; and Institute of Biomedical Engineering, University of Montreal, Montréal H3T-1J4, QC, Canada (guy.cloutier@umontreal.ca).

AMS subject classifications. 62F10, 62H35, 62P10, 62P35, 33C10, 33C20, 33B15

DOI. 10.1137/120875727

1. Introduction.

The homodyned K-distribution appears naturally in the context of a limiting random walk modeling physical scattering process, with a constant-amplitude coherent component and with a negative binomial distribution for the number of steps [13, 15]. As a special case, the K-distribution [21, 14] corresponds to a vanishing coherent component of the amplitude of that process. Also, the Rice distribution corresponds to the limiting case where the scatterer clustering parameter implicit in the negative binomial distribution is infinite [24, 30, 15]. Finally, the Rayleigh distribution [29, 15] corresponds to the Rice distribution with a vanishing coherent component. Both the Rice and the Rayleigh distributions correspond to a Gaussian random walk, but not the homodyned K-distribution (or the K-distribution). The random variable of these distributions is called the amplitude and is denoted by A. The intensity I is defined as the square of the amplitude.

K-distributions and, more generally, homodyned K-distributions turned out to provide a useful model for the received amplitude in a wide range of non-Gaussian scattering configurations, such as optical propagation through turbulent media [27], microwave sea echo [38], land clutter [26], and medical ultrasonics [33, 8, 23, 10, 28, 25]. See [6] for a presentation of the homodyned K-distribution and related distributions in the context of ultrasound imaging.

The homodyned K-distribution is determined by three parameters that carry a physical meaning: the mean intensity μ; the scatterer clustering parameter α (i.e., the clustering parameter in the negative binomial distribution); and the structure parameter κ (i.e., the ratio of the coherent signal power to the diffuse signal power). Given a sample of the received amplitude, one is then interested in estimating those three parameters, or related parameters, such as the signal-to-noise ratio (SNR) of the intensity and the ratio of coherent signal to diffuse signal, denoted k in [8, 11]. The goal is then to use the estimated parameters in the context of tissue characterization or quantitative ultrasound (QUS) based on medical ultrasound images. See [25, 11] as examples.

A simple estimation method of the homodyned K-distribution based on the first three moments of the intensity $E[I]$, $E[I^2]$, and $E[I^3]$ was proposed in [8]. In [11], the SNR, the skewness, and the kurtosis of two fractional orders (namely, 0.72 and 0.88) of the amplitude were used as statistics for the estimation of the homodyned K-distribution. In the case of the estimation method of [11], one obtains an overdetermined nonlinear system of equations that is solved in the sense of the least mean square.

In this paper, an estimation method based on the first moment of the intensity $E[I]$, the U-statistics $E[\log I] - \log E[I]$, and the X-statistics $E[I \log I]/E[I] - E[\log I]$ is proposed. The U- and X-statistics were introduced in the context of K-distributions in [26] and [4], respectively. Moreover, an algorithm with a geometric rate of convergence for the computation of this new estimator is proposed.

The remaining part of this paper is organized as follows. In section 2, the definition of the homodyned K-distribution is recalled. In section 3, the proposed estimation method is explained. Experimental results based on simulations of sample sets and of ultrasound images

Table 1
Main parameters and statistics discussed in this paper.

Definition	Notion
A and $I = A^2$	amplitude and intensity
$\overline{I}$	mean intensity of a sample $A_1, \ldots, A_N$
$U = \overline{\log I} - \log \overline{I}$	U-statistics
$X = \overline{I \log I}/\overline{I} - \overline{\log I}$	X-statistics
Homodyned K-distribution with parameters $\varepsilon \geq 0$, $\sigma^2 > 0$, and $\alpha > 0$	
α	scatterer clustering parameter
ε^2	coherent signal power
$2\sigma^2\alpha$	diffuse signal power
$\mu = \varepsilon^2 + 2\sigma^2\alpha$	total signal power (mean intensity)
$\kappa = \varepsilon^2/(2\sigma^2\alpha)$	structure parameter
$\gamma = \varepsilon^2/(2\sigma^2) = \kappa\alpha$	algorithmic parameter
$k = \sqrt{2\kappa} = \varepsilon/(\sigma\sqrt{\alpha})$	ratio of the coherent to diffuse signal
Rice distribution with parameters $\varepsilon \geq 0$ and $\sigma_{\mathrm{R}}^2 > 0$	
$\mu = \varepsilon^2 + 2\sigma_{\mathrm{R}}^2$	mean intensity
$\kappa = \varepsilon^2/(2\sigma_{\mathrm{R}}^2)$	structure parameter
$k = \sqrt{2\kappa} = \varepsilon/\sigma_{\mathrm{R}}$	ratio of the coherent to diffuse signal

are presented in section 4. The results are discussed in section 5, and we conclude in section 6.

Table 1 presents the definition of the main parameters and statistics discussed in this paper. Given a sample set $\{A_1, \ldots, A_N\}$, the notation $\overline{f(A)}$ denotes the average value of the function f over the sample set, i.e., $\frac{1}{N}\sum_{i=1}^{N} f(A_i)$. In particular, the notation $\overline{I}$, for instance, denotes $\frac{1}{N}\sum_{i=1}^{N} A_i^2$. The notation $\frac{\partial}{\partial\alpha}$ is used for the partial derivative with respect to, say, α. For example, the notation P_{K} does not mean partial derivative, but rather that K is used as a subscript (identifying the K-distribution).

2. The homodyned K-distribution.

The reader is referred to [15] for a presentation of the homodyned K-distribution and the related Rice distribution in the context of random walks, and to [6] for a presentation in the context of ultrasound imaging. The reader may consult [2] for the notions of Bessel functions.

The two-dimensional homodyned K-distribution is defined by

$$P_{\mathrm{HK}}(A \mid \varepsilon, \sigma^2, \alpha) = A \int_0^\infty u\, J_0(u\,\varepsilon) J_0(u\,A) \left(1 + \frac{u^2\sigma^2}{2}\right)^{-\alpha} d\,u, \tag{2.1}$$

where $\varepsilon \geq 0$, $\sigma^2 > 0$, and $\alpha > 0$, and J_0 denotes the Bessel function of the first kind of order 0. The limiting case of a homodyned K-distribution with parameters ε, $\sigma^2 = \sigma_{\mathrm{R}}^2/\alpha$, and α, where $\sigma_{\mathrm{R}}^2 > 0$ is a positive real number and $\alpha \to \infty$, yields the Rice distribution

$$P_{\mathrm{Ri}}(A \mid \varepsilon, \sigma_{\mathrm{R}}^2) = \frac{A}{\sigma_{\mathrm{R}}^2} I_0\left(\frac{\varepsilon}{\sigma_{\mathrm{R}}^2} A\right) \exp\left(-\frac{(\varepsilon^2 + A^2)}{2\sigma_{\mathrm{R}}^2}\right), \tag{2.2}$$

where I_0 denotes the modified Bessel function of the first kind of order 0.

The compound representation of Theorem 2.1 is useful in simulating the homodyned K-distribution and in evaluating its values.

Theorem 2.1 (Jakeman and Tough [15]). *The compound representation of the homodyned K-distribution is*

$$P_{\mathrm{HK}}(A \mid \varepsilon, \sigma^2, \alpha) = \int_0^\infty P_{\mathrm{Ri}}(A \mid \varepsilon, \sigma^2 w) \mathcal{G}(w \mid \alpha, 1) d\, w, \tag{2.3}$$

where $\mathcal{G}(w \mid \alpha, 1) = w^{\alpha-1} e^{-w}/\Gamma(\alpha)$ is the gamma distribution with mean and variance α, and Γ denotes the Euler gamma function.

Two functions of the three parameters of the homodyned K-distribution are invariant under scaling of the *mean intensity* $\mu = \varepsilon^2 + 2\sigma^2\alpha$: (1) the *scatterer clustering parameter* α; (2) the *structure parameter* $\kappa = \varepsilon^2/(2\sigma^2\alpha)$, i.e., the ratio of the *coherent signal power* ε^2 to the *diffuse signal power* $2\sigma^2\alpha$. Let us mention also the *ratio of the coherent to diffuse signal* $k = \sqrt{2\kappa} = \varepsilon/(\sigma\sqrt{\alpha})$ adopted in [8, 11]. It was found convenient to also consider the parameter $\gamma = \kappa\alpha = \varepsilon^2/(2\sigma^2)$. This parameter should not be confused with the structure parameter $\kappa = \varepsilon^2/(2\sigma_{\mathrm{R}}^2)$ of the Rice distribution $P_{\mathrm{Ri}}(A \mid \varepsilon, \sigma_{\mathrm{R}}^2)$. See Table 1 for a summary of these parameters. The special case where $\varepsilon = 0$ yields the K-distribution $P_{\mathrm{K}}(A \mid \sigma^2, \alpha)$ [21, 15] and the Rayleigh distribution $P_{\mathrm{Ra}}(A \mid \sigma_{\mathrm{R}}^2)$ [29].

3. A new method for estimating the homodyned K-distribution. A new method for estimating the parameters $(\varepsilon, \sigma^2, \alpha)$ of the homodyned K-distribution based on an independent and identically distributed (i.i.d.) sample set $(A_1, \ldots, A_N)$ of positive real numbers is now discussed.

Two statistics will play an important role in what follows: (1) the U-statistics defined by $U := \overline{\log I} - \log \overline{I}$ and (2) the X-statistics defined as $X := \overline{I \log I}/\overline{I} - \overline{\log I}$. For parametric models, such as the homodyned K-distribution or the Rice distribution, the U-statistics is defined as $E[\log I] - \log E[I]$, where expectation is taken with respect to the distribution. Similarly, the X-statistics is defined as $E[I \log I]/E[I] - E[\log I]$. A subindex (such as "HK") is then used to identify the distribution (e.g., "U_{HK}").

For later reference, it is instructive to observe the following result.

Lemma 3.1. (a) *For any nonconstant random variable, the U-statistics is negative.*

(b) *For any nonconstant random variable, the X-statistics is positive.*

The proof of Lemma 3.1 is presented in Appendix A.

3.1. Proposed estimator. The proposed method of estimation consists in solving the following (nonlinear) system of equations in the variables ε^2, σ^2, and α:

$$E[I] = \overline{I}, \qquad U_{\mathrm{HK}} = U, \qquad X_{\mathrm{HK}} = X. \tag{3.1}$$

Sufficient conditions for this system to admit a solution are presented below. For this purpose, it will be convenient to adopt the following change of variables:

$$\mu = \varepsilon^2 + 2\sigma^2\alpha, \qquad \gamma = \frac{\varepsilon^2}{2\sigma^2}. \tag{3.2}$$

Proposition 3.2. *Let $A = \sqrt{I}$ be distributed according to the homodyned K-distribution $P_{\mathrm{HK}}(A \mid \varepsilon, \sigma^2, \alpha)$. With the notation of (3.2), one has*

$$\begin{aligned} &U_{\mathrm{HK}}(\gamma,\alpha) \\ &= -\gamma_E - \log(\gamma+\alpha) + \psi(\alpha) \\ &\quad - \gamma^\alpha \frac{\Gamma(-\alpha)}{\alpha\Gamma(\alpha)}\, {}_1F_2(\alpha; 1+\alpha, 1+\alpha; \gamma) + \gamma \frac{\Gamma(\alpha-1)}{\Gamma(\alpha)}\, {}_2F_3(1,1;2,2,2-\alpha;\gamma), \end{aligned} \tag{3.3}$$

$$\begin{aligned} &X_{\mathrm{HK}}(\gamma,\alpha) \\ &= \frac{(1+2\alpha)}{(\gamma+\alpha)} - \frac{2\gamma^{\alpha/2+1/2}}{(\gamma+\alpha)\Gamma(\alpha)} K_{\alpha+1}\left(2\sqrt{\gamma}\right) \\ &\quad + \frac{\gamma^\alpha}{(\gamma+\alpha)} \frac{\Gamma(-\alpha)}{\Gamma(\alpha)}\, {}_1F_2(\alpha; 1+\alpha, 1+\alpha; \gamma) \\ &\quad - \frac{\gamma^{\alpha+1}}{(\gamma+\alpha)} \frac{\Gamma(-1-\alpha)}{(1+\alpha)\Gamma(\alpha)}\, {}_1F_2(1+\alpha; 2+\alpha, 2+\alpha; \gamma) \\ &\quad + \frac{\gamma}{(\gamma+\alpha)}\, {}_2F_3(1,1;2,2,1-\alpha;\gamma) - \frac{\gamma}{(\gamma+\alpha)} \frac{\alpha\Gamma(-1+\alpha)}{\Gamma(\alpha)}\, {}_2F_3(1,1;2,2,2-\alpha;\gamma), \end{aligned} \tag{3.4}$$

where γ_E denotes the Euler constant, ψ is the digamma function, ${}_pF_q(a_1,\ldots,a_p;b_1,\ldots,b_q;z)$ is the generalized hypergeometric series, and K_p denotes the modified Bessel function of the second kind of order p.

As one can see, (3.3) and (3.4) depend only on the variables γ and α. Thus, the proposed method amounts to solving the second and third equations of (3.1) in the variables γ and α, and then using the identities

$$\varepsilon^2 = \mu\gamma/(\gamma+\alpha), \qquad \sigma^2 = \mu/(2(\gamma+\alpha)), \tag{3.5}$$

with the estimator $\overline{I}$ of the mean intensity μ.

The proof of Proposition 3.2 is presented in Appendix A.

3.2. Estimating γ when α is known. Let $\alpha > 0$ be known. A method for finding $\gamma > 0$ satisfying (3.4) is now discussed. Thus, one wants to solve the equation $X_{\mathrm{HK}}(\gamma,\alpha) = X$.

In Appendix B, the following result is shown.

Theorem 3.3. *Use the same notation as above.*

(a) *One has the left boundary condition $\lim_{\gamma\to 0} X_{\mathrm{HK}}(\gamma,\alpha) = X_{\mathrm{K}}(\alpha)$, where $X_{\mathrm{K}}(\alpha) = 1 + 1/\alpha$.*

(b) *One has the right boundary condition $\lim_{\gamma\to\infty} X_{\mathrm{HK}}(\gamma,\alpha) = 0$.*

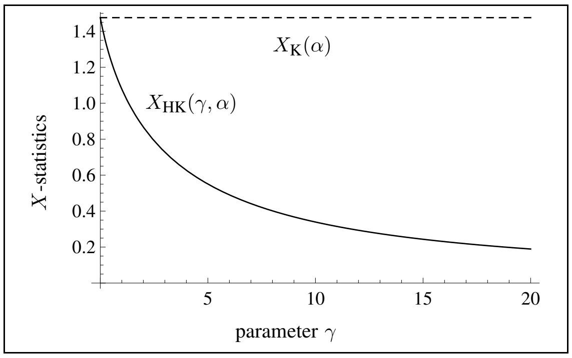

Figure 1. *Illustration of the typical behavior of the X-statistics for the homodyned K-distribution as a function of $\gamma \geq 0$ with a fixed value of $\alpha > 0$ (here, $\alpha = 2.1$).*

(c) *For any $\alpha > 0$, the function $X_{\mathrm{HK}}(\gamma, \alpha)$ is decreasing in the variable γ.*

See Figure 1 for an illustration of Theorem 3.3. Part (c) of Theorem 3.3 implies that a binary search algorithm can be used to find the unique solution to (3.4), whenever it exists. See section 3.4 for details.

Corollary 3.4. *Let $X > 0$. Then, there is at most one solution to the equation $X_{\mathrm{HK}}(\gamma, \alpha) = X$.*

(a) *If $X \leq 1$, then there is a solution for any $\alpha > 0$.*

(b) *If $X > 1$, then there is a solution if and only if $0 < \alpha \leq \alpha_0$, where $\alpha_0 = X_{\mathrm{K}}^{-1}(X) = 1/(X-1)$.*

Thus, one obtains a well-defined function

$$\gamma = \gamma(\alpha, X) \tag{3.6}$$

on the domain described by Corollary 3.4.

3.3. Estimating γ and α. From Corollary 3.4, one knows that for any α in an interval of the form $(0, \alpha_0]$ or $(0, \infty)$, there exists a unique solution $\gamma = \gamma(\alpha, X)$ to the equation $X_{\mathrm{HK}}(\gamma, \alpha) = X$. Substituting this solution in the second equation of (3.1), one obtains a function $U_{\mathrm{HK}}(\gamma(\alpha, X), \alpha)$ in the variable α. Thus, one now wants to solve the equation $U_{\mathrm{HK}}(\gamma(\alpha, X), \alpha) = U$.

See Appendix C for a proof of the following result.

Theorem 3.5. *Let $X > 0$.*

(a) *One has the left boundary condition $\lim_{\alpha \to 0} U_{\mathrm{HK}}(\gamma(\alpha, X), \alpha) = 0$.*

(b) *Let $X > 1$. One has the right boundary condition $\lim_{\alpha \to \alpha_0} U_{\mathrm{HK}}(\gamma(\alpha, X), \alpha) = U_{\mathrm{K}}(\alpha_0)$, where $U_{\mathrm{K}}(\alpha) = -\gamma_E - \log \alpha + \psi(\alpha)$, $X_{\mathrm{K}}(\alpha) = 1 + 1/\alpha$, and $\alpha_0 = X_{\mathrm{K}}^{-1}(X) = 1/(X-1)$.*

(c) *Let $X \leq 1$. One has the right boundary condition $\lim_{\alpha \to \infty} U_{\mathrm{HK}}(\gamma(\alpha, X), \alpha) = U_{\mathrm{Ri}}(\kappa_0)$, where $U_{\mathrm{Ri}}(\kappa) = \Gamma(0, \kappa) + \log \frac{\kappa}{(\kappa+1)}$, $X_{\mathrm{Ri}}(\kappa) = \frac{(2-e^{-\kappa})}{(\kappa+1)}$, and $\kappa_0 = X_{\mathrm{Ri}}^{-1}(X)$. The function $X_{\mathrm{Ri}}(\kappa)$ is decreasing and has the interval $(0, 1]$ for range.*

Since the function $X_{\mathrm{Ri}}(\kappa)$ is decreasing on its domain $[0, \infty)$ and has range $(0, 1]$, the function $X_{\mathrm{Ri}}^{-1}(X)$ is well defined on the interval $X \in (0, 1]$.

Conjecture 1. *The function $U_{\mathrm{HK}}(\gamma(\alpha, X), \alpha)$ is decreasing on its domain.*

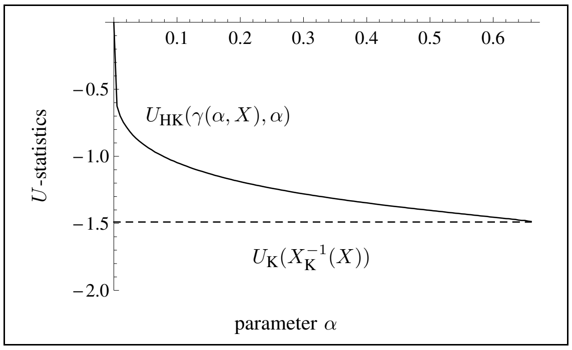

Figure 2. *Illustration of the typical behavior of the U-statistics for the homodyned K-distribution as a function of $\alpha > 0$, with a fixed value of $X > 0$ and $\gamma = \gamma(\alpha, X)$. Here, $X = 2.5$. Since $X > 1$, the upper bound for α is $\alpha_0 = 1/(X - 1)$.*

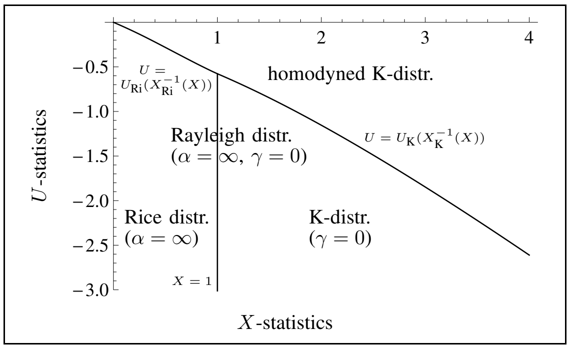

Figure 3. *Illustration of the domain in the (X, U)-plane in which the parameters $\gamma \geq 0$ and α are well defined. The domains where either the K-distribution, the Rice distribution, or the Rayleigh distribution model apply are also indicated. The Rayleigh distribution corresponds to the vertical line.*

See Figure 2 for an illustration of Theorem 3.5 and the conjecture. The conjecture implies that a binary search algorithm can be used to find the unique solution to the second and third equations of (3.1), whenever a solution exists. The details are presented in section 3.4. In Appendix D, a discussion on Conjecture 1 is presented.

Combining Theorems 3.3 and 3.5 with the conjecture yields the following result.

Corollary 3.6. *Let $U < 0$ and $X > 0$ be given. Then, there exists a simultaneous solution to the system $U_{\rm HK}(\gamma, \alpha) = U$ and $X_{\rm HK}(\gamma, \alpha) = X$ if and only if*

(a) *$X > 1$ and $U > U_{\rm K}(X_{\rm K}^{-1}(X))$, or*

(b) *$X \leq 1$ and $U > U_{\rm Ri}(X_{\rm Ri}^{-1}(X))$.*

Moreover, if a solution exists, it is unique.

Thus, one obtains well-defined functions

$$\gamma = \gamma(X, U), \qquad \alpha = \alpha(X, U), \tag{3.7}$$

where X and U are restricted to the domain described by parts (a) and (b) of Corollary 3.6. See Figure 3 for an illustration of this domain.

| $X_{\mathrm{HK}}(\gamma, \alpha)$ function of (3.4);

Input: $X > 0$ (the X-statistics) and $\alpha > 0$.
Assumption: $\alpha \le \alpha_0 = 1/(X-1)$ if $X > 1$; no restriction if $0 < X \le 1$.

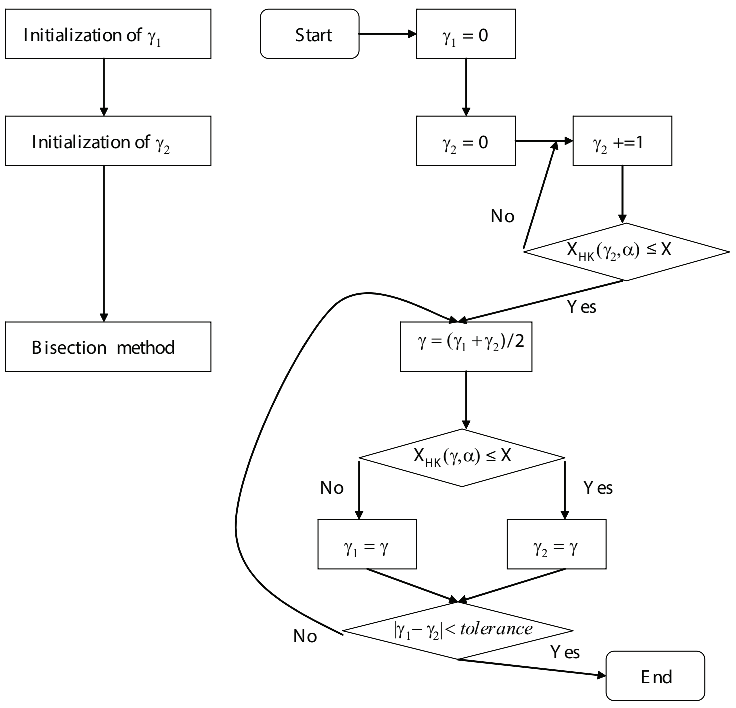

Figure 4. *Algorithm for computing the function $\gamma(\alpha, X)$ of (3.6). Left: block diagram; right: flow chart.*

3.4. Algorithms for solving the system (3.1). The algorithm presented in Figure 4 is used as a subroutine in the algorithm of Figure 5 that computes the unique solution (according to Conjecture 1) to the system (3.1), whenever U and X satisfy the conditions of Corollary 3.6.

First of all, Figure 4 gives a binary search algorithm for computing the function $\gamma(\alpha, X)$ of (3.6) (α being known) by solving the equation $X_{\mathrm{HK}}(\gamma, \alpha) = X$. Since (from Theorem 3.3) the function $X_{\mathrm{HK}}(\gamma, \alpha)$ is decreasing in the variable γ and since (by assumption) X is between the upper bound $X_{\mathrm{K}}(\alpha) = 1 + 1/\alpha$ and the lower bound 0, it follows that the algorithm of Figure 4 converges to the unique solution of the equation $X_{\mathrm{HK}}(\gamma, \alpha) = X$, as follows from the intermediate value theorem. Note that this binary search algorithm corresponds to the bisection method [9] and converges at a geometric rate; namely, after each iteration the distance between the current value of γ and the solution decreases by a factor of 2.

Having this algorithm as a tool, one can solve the equation $U_{\mathrm{HK}}(\gamma(\alpha, X), \alpha) = U$ using the binary search algorithm of Figure 5 for reasons similar to those above, based on Conjecture 1.

| $U_{\mathrm{HK}}(\gamma,\alpha)$ function of (3.3);
| $\gamma(\alpha,X)$ function computed by the algorithm of Figure 4.

Input: $X > 0$ and $U < 0$ (the X- and U-statistics).
Assumption: $X > 1$ and $U > U_{\mathrm{K}}(\alpha_0)$, where $\alpha_0 = 1/(X-1)$; OR $0 < X \leq 1$ and $U > U_{\mathrm{Ri}}(X_{\mathrm{Ri}}^{-1}(X))$.

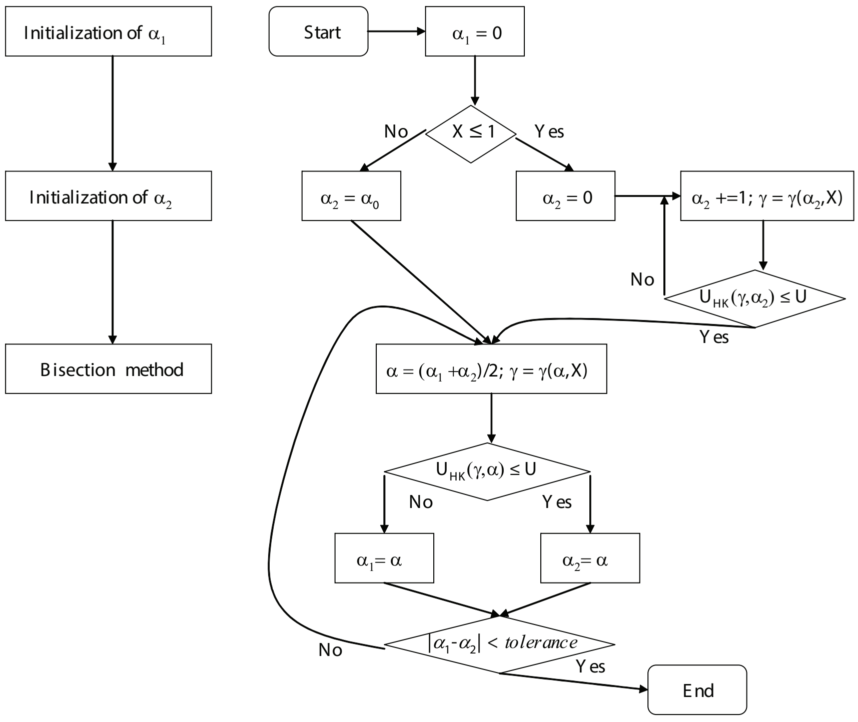

Figure 5. *Algorithm for solving simultaneously $X_{\mathrm{HK}}(\gamma,\alpha) = X$ and $U_{\mathrm{HK}}(\gamma,\alpha) = U$. Left: block diagram; right: flow chart.*

Indeed, according to the conjecture, the function $U_{\mathrm{HK}}(\gamma(\alpha,X),\alpha)$ is decreasing, and Theorem 3.5 gives the upper and lower bounds of that function. Note that the assumptions on X and U of the algorithm are those of Corollary 3.6. Moreover, observe that the assumption of the subroutine of Figure 4 is satisfied whenever it is called in the algorithm of Figure 5. Details on the computation of the functions X_{HK} and U_{HK} are given in Appendix E. Since the value of $\gamma = \gamma(\alpha,X)$ is computed for each value of α considered in the algorithm of Figure 5, an error on that computation propagates on the error in the estimation of α. So, one has to allow enough precision. In the implementation of the reported tests, we adopted a tolerance of 10^{-4} and 10^{-2} in the algorithms of Figures 4 and 5, respectively.

3.5. Overall algorithm. We now discuss an extension of the above method in the case where the system (3.1) has no solution, i.e., whenever U and X do not satisfy the conditions of Corollary 3.6. Also, there is a further issue on the size of α with respect to numerical considerations. On that matter, one has to know that the various functions appearing in the expression of $X_{\rm HK}$ and $U_{\rm HK}$ (such as the digamma function) have a finite support in any implementation. Therefore, in practice, one has to limit the size of α to a finite interval $(0, \alpha_{\max}]$. So, we resort to the algorithm of Figure 6 for a practical implementation of the proposed approach. This algorithm finds a solution to the system

$$(\varepsilon, \sigma^2, \alpha) = \arg\min |U_{\rm HK} - U| \quad \text{subject to } \mu = \overline{I} \text{ and } X_{\rm HK} = X \text{ and } \alpha \le \alpha_{\max}, \tag{3.8}$$

as follows directly from Conjecture 1 (i.e., the function $U_{\rm HK}(\gamma(\alpha, X), \alpha)$ is decreasing in the variable α). Observe that a solution to the system (3.1) such that $\alpha \le \alpha_{\max}$ is automatically a solution to the system (3.8). Note that in the algorithm of Figure 6, a homodyned K-distribution with parameters ε, σ^2, $\alpha > \alpha_{\max}$ is approximated by the distribution with parameters

$$\tilde{\varepsilon} = \sqrt{\mu \frac{\tilde{\gamma}}{(\tilde{\gamma} + \alpha_{\max})}}, \quad \tilde{\sigma}^2 = \frac{\mu}{2\alpha_{\max}(\tilde{\gamma} + \alpha_{\max})}, \quad \alpha_{\max}, \tag{3.9}$$

where $\tilde{\gamma} = \gamma(\alpha_{\max}, X_{\rm HK}(\frac{\varepsilon^2}{2\sigma^2 \alpha}, \alpha))$.

In the reported tests, we chose $\alpha_{\max} = 59.5$, i.e., as large as possible but within a range for which the various functions used in the C++ implementation of the method could be supported numerically. In view of the numerical behavior of the function $X_{\rm HK}$ at integral values of α (see Appendix E), one might as well choose an odd integer divided by 2 for the value of $\alpha_{\max}$. Finally, we have checked numerically that the Kullback–Leibler distance [20] between a homodyned K-distribution with parameters ε, σ^2, α and the distribution with parameters as in (3.9) is less than 1.8×10^{-4} for parameter values in the range $k = \frac{\varepsilon}{\sigma\sqrt{\alpha}} \in \{0, 0.1, \dots, 1.9, 2.0\}$ and $\alpha, \alpha_{\max} \in \{59.5, 61.5, \dots, 79.5\}$. Note that the Kullback–Leibler distance is independent of the scaling factor μ, so that we assumed $\mu = 1$ in the numerical computations. Thus, we are inclined to think that a homodyned K-distribution with $\alpha > \alpha_{\max}$ is approximated sufficiently well by the algorithm of Figure 6 and that the choice of $\alpha_{\max} \ge 59.5$ is not crucial, at least if $k \le 2$. However, we do not have a proof of this hypothesis because the analytical computations appeared to be intractable.

3.6. Are k and α the right parameters to estimate? The biases and normalized standard deviations reported in [11] are rather high. For instance, from [11, Figure 3], the relative biases for k and α go up to about 600% and 100%, respectively, and their normalized standard deviations reach about 300%. This suggests that one should consider a transformation of these parameters. In [8], the parameter $\beta = 1/\alpha$ is considered rather than α itself. For one estimation, the two solutions are equivalent, but for numerous estimations, the biases and standard deviations are not necessarily equivalent, because the averaging operator is not invariant under a transformation unless that transformation is linear. Thus, for instance, the relative bias of $1/\alpha$ might be lower than the relative bias of α.

In this study, the parameters $1/(\kappa + 1)$ and $1/\alpha$ were adopted. As will be presented in section 4.1, the relative biases and normalized standard deviations were improved considerably with that choice of transformations. So, in the applications considered, the parameters $1/(\kappa+$

$U_{\mathrm{HK}}(\gamma,\alpha)$	function of (3.4);
$\gamma(\alpha, X)$	function computed by the algorithm of Figure 4.
$\alpha_{\max}$	upper bound on α.

Input: $\bar{I} > 0$ (the mean intensity), $X > 0$ and $U < 0$ (the X- and U-statistics).

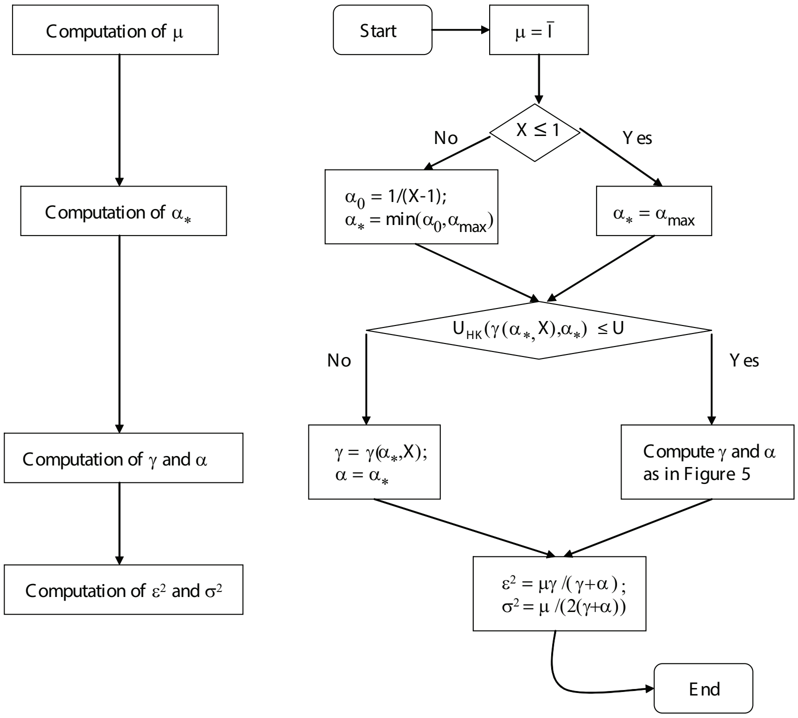

Figure 6. *Algorithm for estimating the parameters ε^2, σ^2, α of the homodyned K-distribution with the constraint that α is less than an upper bound $\alpha_{\max}$. Left: block diagram; right: flow chart.*

1) and $1/\alpha$ are estimated in each frame of a sequence of ultrasound images, and those estimated values are then averaged out over all frames. See section 4.2 for such an application.

The advantage of the proposed choice of parameters is that, even if $\alpha = \infty$ (corresponding to the Rice model), the parameter $1/\alpha$ has a meaningful finite value (namely 0). In fact, the parameters $1/(\kappa+1)$ and $1/\alpha$ have values within the intervals $(0, 1]$ and $[0, \infty)$, respectively, even in the case of the Rice, Rayleigh, or K-distribution model. See section 5.6 for further discussion on this issue.

4. Experimental results.

4.1. Comparison of estimators based on simulation of data samples. In order to compare the reported experimental results with those of [11], it was decided to present the results in terms of the scatterer clustering parameter α and the ratio of coherent to diffuse signal $k = \sqrt{2\kappa}$, where $\kappa = \varepsilon^2/(2\sigma^2\alpha)$ is the structure parameter. Following the same approach as in [11], 100 sets of values of the parameters k and α were considered in the domains

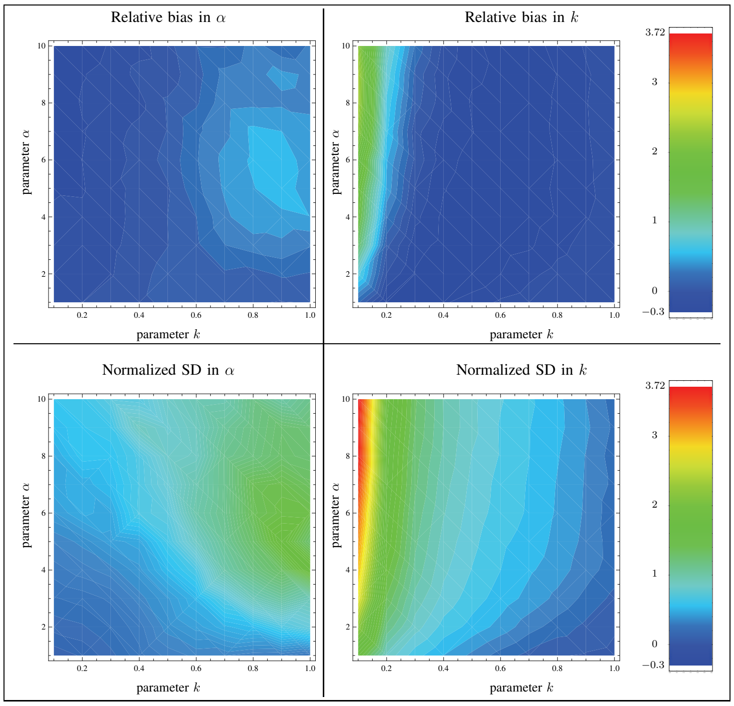

Figure 7. *Relative bias and normalized standard deviation (SD) of the parameter estimates based on the XU estimator. The sample size is $N = 1000$. The computation of the biases and standard deviations excluded the instances where α was greater than $\alpha_{\max}$.*

$k \in \{0.1, 0.2, \ldots, 0.9, 1.0\}$ and $\alpha \in \{1, 2, \ldots, 9, 10\}$, and the value of σ^2 was taken as $1/\alpha$, so that the diffuse signal power $2\sigma^2\alpha = 2$ was kept constant. For each of these sets, 1000 samples of size $N = 1000$ each were simulated, according to the homodyned K-distribution model. The parameters from each sample were then estimated using (1) the moments of intensity method [8] (MI), (2) a method based on the first three moments of the amplitude (MA), (3) the proposed method based on the mean intensity and the X- and U-statistics (XU), and (4) the method [11] based on the SNR, skewness, and kurtosis of two fractional orders of the amplitude (RSK). For each estimation method, the relative biases $(E[\hat{k}] - k)/k$ and $(E[\hat{\alpha}] - \alpha)/\alpha$, the normalized standard deviations $\sqrt{Var[\hat{k}]}/k$ and $\sqrt{Var[\hat{\alpha}]}/\alpha$, and the relative root mean squared errors (RMSEs) defined by $\sqrt{E[(\hat{k} - k)^2]}/k$ and $\sqrt{E[(\hat{\alpha} - \alpha)^2]}/\alpha$ were computed, based on the 1000 estimates $\hat{k}$ and $\hat{\alpha}$ of those parameters. The relative bias and normalized standard deviation of the proposed estimator are presented in Figure 7. As in [11], the computation of the bias and standard deviation did not include the instances where α was outside a reasonable range (i.e., $\alpha \geq 59.5$ for the MI, MA, and XU methods). In Table 2, the sums of the quantities represented in Figure 7 over the sets of parameters that were considered are presented for each of the tested methods. See Appendix F for the implementation of the MI method in the reported tests. The implementation of the MA method follows a strategy similar to that presented in section 3. We decided to skip the details in the current paper since the MA method performed less well than the proposed estimator. For the MI and

Table 2

Improvements in bias and variance of estimators. The sample size is $N = 1000$. Estimation methods: (1) MI [8]; (2) MA; (3) XU (proposed method); (4) RSK [11]. The computation of the biases and standard deviations excluded the instances where α was greater than $\alpha_{\max}$ for the MI, MA, XU methods. A star (*) indicates the best relative RMSE value among the four estimators.

	MI	MA	XU	RSK
Total absolute value of the relative bias of $\hat{\alpha}$	47.9	19.6	17.5	23.9
Total absolute value of the relative bias of $\hat{k}$	42.2	33.2	34.7	60.7
Total normalized standard deviation of $\hat{\alpha}$	108.9	73.7	70.3	84.5
Total normalized standard deviation of $\hat{k}$	117.0	92.0	91.1	62.1
Total value of the relative RMSE of $\hat{\alpha}$	120.3	76.7	72.7*	88.2
Total value of the relative RMSE of $\hat{k}$	126.6	99.1	99.1	92.7*

Table 3

Relative RMSE of estimators for various parameters of the homodyned K-distribution. The sample size is $N = 1000$. Estimation methods: (1) MI [8]; (2) MA; (3) XU (proposed method); (4) RSK [11]. For the MI, MA, XU methods, the computation of the biases and standard deviations did not exclude any values of α, because $1/\alpha = 0$ is a solution. A star (*) indicates the best MSE value among the four estimators.

	MI	MA	XU	RSK
Mean relative RMSE of $\hat{\alpha}$	1.69	1.06	1.04	0.88*
Mean relative RMSE of $\widehat{1/\alpha}$	1.37	0.64	0.63*	0.67
Mean relative RMSE of $\hat{k}$	1.26	0.99	0.99	0.93*
Mean relative RMSE of $\hat{\kappa}$	6.90	4.29*	4.37	4.87
Mean relative RMSE of $\widehat{\sqrt{2\gamma}}$	1.04	0.86	0.85*	0.88
Mean relative RMSE of $\widehat{1/(\kappa+1)}$	0.18	0.12	0.13	0.11*

MA methods, a minimization problem similar to (3.8) is considered to circumvent the case where the system of nonlinear equations has no solution.

Next, the relative RMSEs of the various tested estimators were evaluated for the parameters k and α, as well as the parameters κ, $\sqrt{2\gamma} = \varepsilon/\sigma$, $1/(\kappa + 1)$, and $1/\alpha$, but without excluding high values of α for the MI, MA, and XU methods (since $1/\alpha = 0$ is a solution). The results are presented in Table 3.

4.2. Estimation based on simulated ultrasound images.

4.2.1. Experimental set-up. The reported computational simulations were inspired by the work of [11, section III-D-2]. Namely, radiofrequency (RF) data were simulated using the Field II ultrasound simulation program [18, 17]. A single-element oscillating focused (f/4) transducer with a focal length of 50.8 mm was used. Its center frequency was 10 MHz, and it was excited with a Gaussian windowed sinusoidal pulse with a 50% fractional bandwidth at −6 dB. The excitation pulse length was 0.616 mm, i.e., four times the wavelength (that information is missing from [11]). The sampling frequency was 200 MHz, and the scan lines to produce an image were separated by 0.43 mm. The speed of sound was equal to 1540 m/s. These choices amount to an axial and a lateral discretization of 0.00385 mm and 0.43 mm per pixel, respectively. As in [11], no tissue attenuation was added in these simulations. The ultrasound echo envelope was computed as the norm of the Hilbert transform of the RF data (see [19]). The resulting unfiltered and uncompressed B-mode image was then decimated along the beam axis by a factor of 10 in order to have an i.i.d. sample modeled by a single homodyned K-distribution.

A computational phantom of height 17.2 mm, length 20.7 mm, and width 1.72 mm was also considered. The center of the volume was located at the geometric focus of the transducer. The resolution cell (a volume which corresponds to the smallest resolvable detail [5]) was obtained by scanning one scatterer located at the geometric focus of the transducer and considering the -20 dB contour of the echo envelope (as in [8]). The resolution cell size was then estimated using the correlation length method (as in [8]) along the axial and lateral directions. The resolution cell volume (based on an ellipsoid model) was 0.2153 mm^3 (the ellipsoid semiprincipal axis in the beam direction measured 0.2180 mm, and the two other semiprincipal axes were 0.4856 mm long). Thus, a density (i.e., average number of scatterers per unit volume) of N_s scatterers per resolution cell corresponded to $N_s \times 2844$ scatterers within the numerical phantom (N_s was variable in the reported tests).

4.2.2. Variation of the density of randomly located scatterers. Randomly located scatterers were placed in the phantom volume at spatial locations distributed according to a uniform distribution. The amplitude of each scatterer (related to the contrast in acoustic impedance between the scatterer and the surrounding medium) was distributed according to a normal distribution of mean 0 and variance 1, as in [17] (this information is missing in [11]). Sequences of ultrasound images were simulated with an average number of randomly located scatterers per resolution cell varying from 1 to 10 (for a total of 10 simulated sequences). For each value of the scatterer density, a total of 60 images were simulated. See Figure 8 for examples of simulated images.

For each simulated sequence, the estimated values of $1/(\kappa+1)$ and $1/\alpha$ were averaged over the 60 images of the sequence within a region of interest (ROI), based on the XU estimator. The ROI consisted of the rectangle covered by 6 resolution cells in the axial direction and about 35 resolution cells in the lateral direction (for a sample size of $N = 13299$ pixels), centered at the geometric focus of the transducer. In Figure 9, the theoretical and estimated values (with the XU estimator) of these parameters are presented. For the theoretical values, the parameter $1/(\kappa + 1)$ should be equal to 1, since there are no periodic scatterers in this simulation (see section 4.2.3). Also, the parameter $1/\alpha$ should be inversely proportional to the number of randomly located scatterers per resolution cell. In fact, from [33, eq. (4)], the parameter α is of the form $\alpha_s N_s$, where N_s is the number of randomly located scatterers per resolution cell and $\alpha_s > 0$ is related to the homogeneity of the scattering cross-sections. Thus, one obtains $1/\alpha = 1/(\alpha_s N_s)$. The constant $1/\alpha_s$ was obtained with the Blacknell–Tough estimator [4], assuming a K-distribution. Namely, for each simulated sequence, corresponding to an average of $i = 1, \ldots, 10$ randomly located scatterers per resolution cell, the estimated value of $1/\alpha_{[i]}$ was averaged over the 60 images. Then, the average $\frac{1}{10}\sum_{i=1}^{10} i/\alpha_{[i]}$ was considered as the constant $1/\alpha_s$ (because the index i in the sum represents N_s). In the reported tests, a value of $1/\alpha_s = 2.243$ was obtained in that manner.

4.2.3. Variation of the coherent component. A fixed density of 3 randomly located scatterers per resolution cell was considered. Coherent scattering was created by using periodically spaced scatterers along the transducer axis. So, their coordinates in the plane perpendicular to the transducer axis were random, whereas their coordinates along that axis were separated by a distance of around $\lambda/2$, where λ is the wavelength. This corresponds to a subresolvable periodic alignment of scatterers. The amplitude of the periodic scatterers was fixed to the constant 1 for each simulation of 60 images, in order to match the average intensity value of the randomly located scatterers. Indeed, the amplitude of the randomly located scatterers

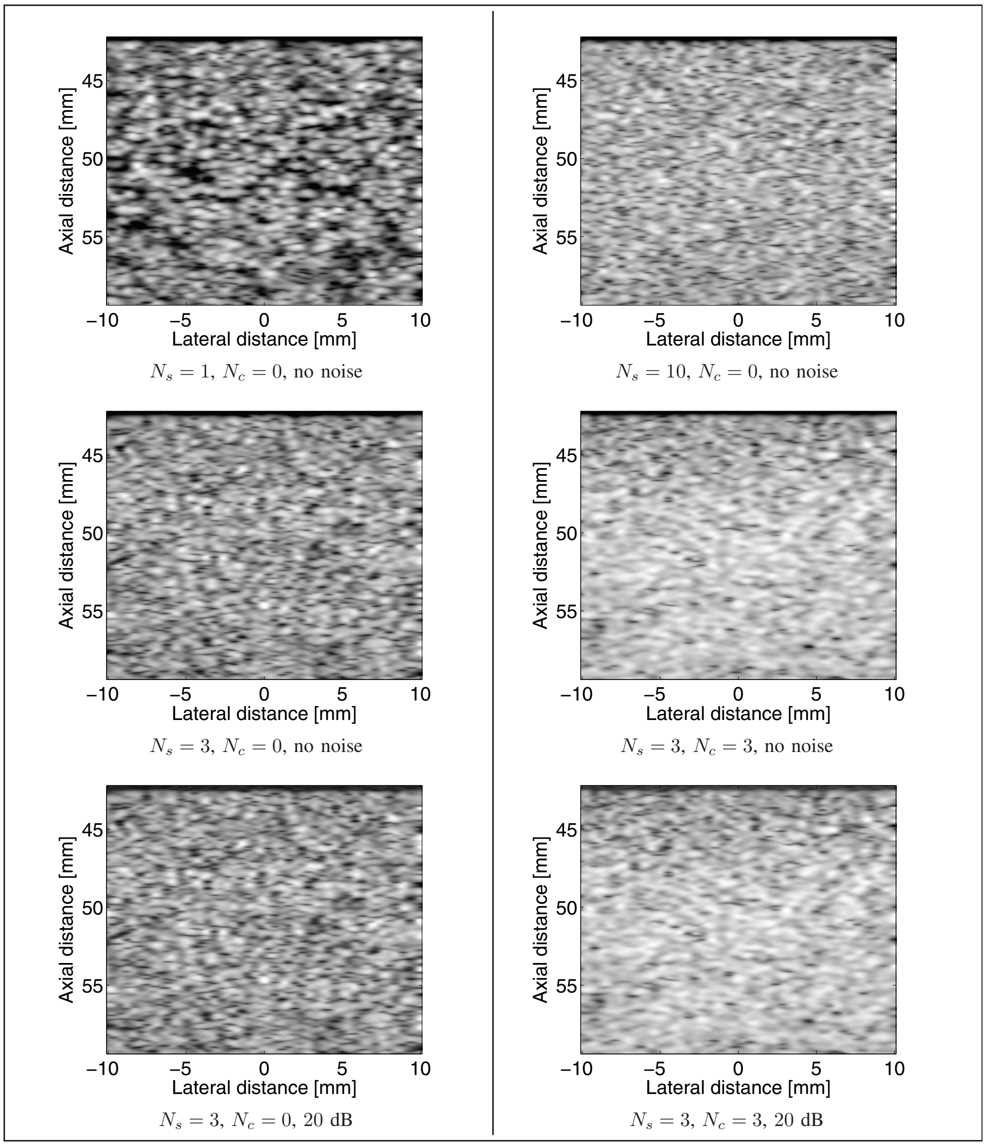

Figure 8. *Examples of simulated B-mode images with N_s randomly located scatterers per resolution cell, and N_c periodic scatterers per resolution cell, with or without noise added to the RF signal. Top left: $N_s = 1$, $N_c = 0$, no noise. Top right: $N_s = 10$, $N_c = 0$, no noise. Middle left: $N_s = 3$, $N_c = 0$, no noise. Middle right: $N_s = 3$, $N_c = 3$, no noise. Bottom left: $N_s = 3$, $N_c = 0$, RF SNR of 20 dB. Bottom right: $N_s = 3$, $N_c = 3$, RF SNR of 20 dB. A log-compression was applied to the echo envelope solely for visualization purposes.*

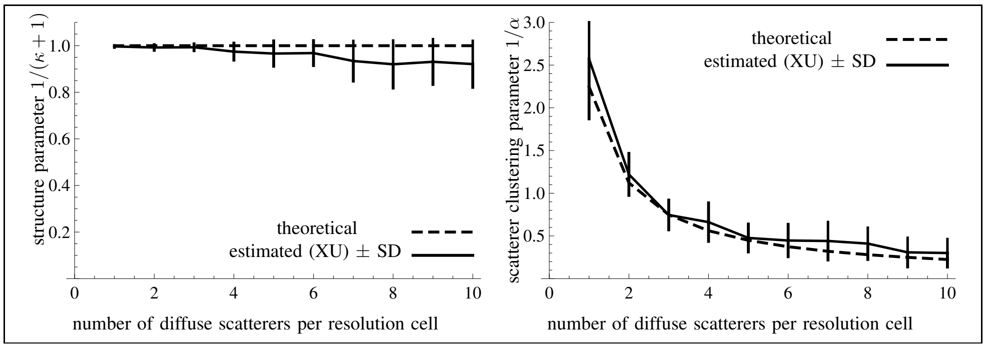

Figure 9. *Values of the parameter $1/(\kappa+1)$ (left) and of the scatterer clustering parameter $1/\alpha$ (right) as a function of the average number of randomly located scatterers per resolution cell. No coherent component was included in these simulations. The sample size of each frame is 13299, and the number of frames is $N = 60$ (used for the computation of the standard deviations). The computation of the biases and standard deviations did not exclude any values of α, because $1/\alpha = 0$ is a possible solution.*

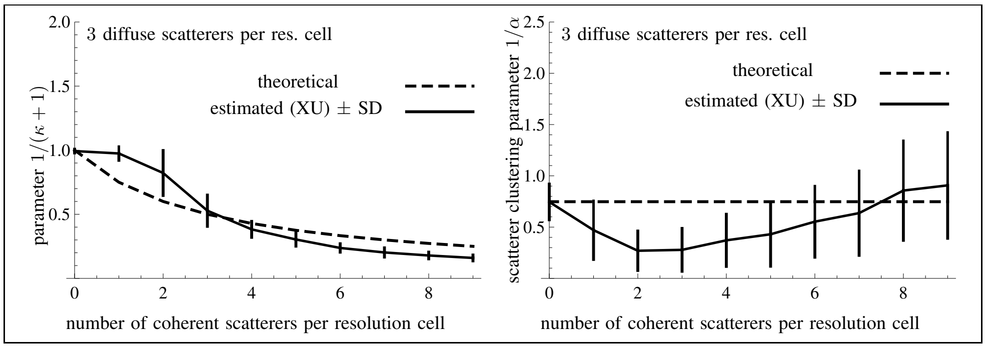

Figure 10. *Values of the parameter $1/(\kappa+1)$ (left) and of the scatterer clustering parameter $1/\alpha$ (right) as a function of the number of coherent scatterers per resolution cell. The sample size of each frame is 13299, and the number of frames is $N = 60$ (used for the computation of the standard deviations). The computation of the biases and standard deviations did not exclude any values of α, because $1/\alpha = 0$ is a possible solution.*

was distributed according to a Gaussian distribution of mean 0 and variance 1, which implies a Rayleigh distribution of mean 1 for the intensity (i.e., the square of the amplitude). The average number of periodic scatterers per resolution cell (i.e., their density) varied from 0 to 9 (with a step of 1), for a total of 10 simulations of 60 images each.

For each simulated sequence, the estimated values of $1/(\kappa + 1)$ and $1/\alpha$ were averaged over the 60 images of the sequence within the ROI of section 4.2.2. In Figure 10, the theoretical and estimated values of these parameters (with the XU method) are presented. As a first approximation, the theoretical value of κ is equal to the ratio of periodic to randomly located scatterers. Moreover, one would expect that the theoretical value of α is constant and corresponds to a density of 3 randomly located scatterers per resolution cell (and no periodic scatterers) times the constant α_s of section 4.2.2. Hence, it can be deduced as in that section.

4.2.4. Presence of noise. The simulations of sections 4.2.2 and 4.2.3 were repeated with the addition of noise on the RF signals (prior to the computation of the echo envelope) to

Table 4

Improvements in mean relative RMSE, mean coefficient of variation (CV) and mean root Fisher's J criterion (RFJC) of estimators. The sample size of each frame is 13299*, and the number of frames is* $N = 60$ *(used for the computation of the standard deviations). Estimation methods:* (1) *MI* [8]; (2) *MA;* (3) *XU (proposed method);* (4) *RSK* [11]*. For the methods MI, MA, and XU, the computation of the biases and standard deviations did not exclude any values of* α*, because* $1/\alpha = 0$ *is a solution. A star* (*) *indicates the best relative RMSE, CV, or RFJC value among the four estimators.*

	Simulations of section 4.2.2					Simulations of section 4.2.3			
Method	MI	MA	XU	RSK		MI	MA	XU	RSK
	No noise					No noise			
Rel. RMSE of $\widehat{1/\alpha}$	0.79	0.61	0.53*	0.67	CV of $\widehat{1/\alpha}$	0.99	0.65	0.61*	0.75
Rel. RMSE of $\widehat{1/(\kappa+1)}$	0.074	0.075	0.069*	0.100	RFJC of $\widehat{1/\kappa+1}$	4.37	5.27	5.73*	3.95
	RF SNR of 20 dB					RF SNR of 20 dB			
Rel. RMSE of $\widehat{1/\alpha}$	0.80	0.62	0.53*	0.67	CV of $\widehat{1/\alpha}$	0.99	0.65	0.61*	0.74
Rel. RMSE of $\widehat{1/(\kappa+1)}$	0.074	0.075	0.069*	0.100	RFJC of $\widehat{1/\kappa+1}$	4.37	5.25	5.78*	3.97
	RF SNR of 10 dB					RF SNR of 10 dB			
Rel. RMSE of $\widehat{1/\alpha}$	0.83	0.66	0.56*	0.70	CV of $\widehat{1/\alpha}$	0.99	0.64	0.61*	0.76
Rel. RMSE of $\widehat{1/(\kappa+1)}$	0.076	0.078	0.071*	0.101	RFJC of $\widehat{1/\kappa+1}$	4.31	5.04	5.54*	3.96
	RF SNR of 5 dB					RF SNR of 5 dB			
Rel. RMSE of $\widehat{1/\alpha}$	0.89	0.72	0.61*	0.76	CV of $\widehat{1/\alpha}$	0.98	0.67	0.61*	0.78
Rel. RMSE of $\widehat{1/(\kappa+1)}$	0.080	0.085	0.077*	0.107	RFJC of $\widehat{1/\kappa+1}$	4.11	4.55	5.03*	3.99

create RF signals with SNRs of 20 dB, 10 dB, or 5 dB. Namely, an SNR of n dB on the RF signal was simulated by adding to the RF signal a Gaussian noise of mean 0 and of variance τ^2 equal to $10^{-n/10} E[I_{\mathrm{RF}}]$, where I_{RF} denotes the square of the RF signal. In this manner, the SNR of the RF signal was equal to $E[I_{\mathrm{RF}}]/\tau^2 = 10^{n/10}$, which indeed corresponds to n dB. A comparison with the simulations with no added noise is presented in Table 4. Four methods were tested: (1) the MI method [8]; (2) the MA method; (3) the XU (proposed) method; and (4) the RSK method [11]. The relative RMSEs are reported in Table 4. Note that the value of the constant $1/\alpha_s$ of section 4.2.2 has to be evaluated for each level of noise. We obtained the values 2.225, 2.106, and 1.896 for SNRs of 20 dB, 10 dB, and 5 dB, respectively.

5. Discussion.

5.1. Comparison of estimators based on simulations of data samples.

As can be seen from Table 2, the XU method for the homodyned K-distribution yielded the lowest total relative RMSE for the parameter α. On the other hand, the total relative RMSE for the parameter k was lowest with the RSK method, whereas the MA and XU methods ranked second.

Note that the values obtained for α and k with the RSK method agree with [11, Table 1]. The values obtained for α with the MI method agree with [11, Table 1], but not the values obtained for k. This is explained by the fact that in the present study, as well as in [11], estimated values were excluded when α was outside its range. However, in [11], estimated values were excluded whenever α was outside its domain for either method [8] or [11]. In the current study, estimated values were excluded for a given estimator only if α was outside its domain for that estimator. We proceeded in that manner in order to test the performance of each method as it stands alone.

Moreover, Table 3 indicates clearly that it is preferable to estimate the parameters $1/(\kappa+1)$ and $1/\alpha$ rather than k (or κ or $\sqrt{2\gamma}$) and α. The XU method yielded a lower relative RMSE than the MI method, whereas it was barely better than the MA method for the parameters α, $1/\alpha$, and $\sqrt{2\gamma}$. On the other hand, the reported tests on simulated images indicate that the XU estimator is preferable to the MA estimator. The RSK method presented the lowest relative RMSE for the parameters α, k, and $1/(\kappa+1)$, but the XU method was best for the parameters $1/\alpha$ and $\sqrt{2\gamma}$.

5.2. Estimation based on simulated ultrasound images.

5.2.1. Variation of the density of randomly located scatterers. Table 4 (left part) shows that the XU estimation method performs better than the other tested methods. These results are in agreement with the RMSEs obtained on simulated data samples of section 4.1, as far as the XU and RSK methods are concerned. On the other hand, the XU method appears to be much better than the MA method on simulated images, whereas the tests performed on simulated data samples did not stress this fact. This is explained by the fact that the X- and U-statistics arise in the limiting case where the fractional exponent of the fractional moment estimator is small [4] (i.e., near 0 or 1), since higher order moments are more sensitive to noise. Note that the estimates improve in the presence of less noise on the RF signal.

As can be seen from Figure 9, the estimation of the parameters $1/(\kappa+1)$ and $1/\alpha$ is reliable up to 3 scatterers per resolution cell ($1/\alpha > 0.7$) in the context of the reported tests. This is due to the behavior of the estimator for large values of α when $\kappa = 0$. Namely, the normalized bias and standard deviation of the estimator of $k = \sqrt{2\kappa}$ increase with the size of α, as can be seen from Figure 7 (right side) on the axis $k = 0$. Moreover, the normalized standard deviation of the estimator of α increases with the size of α (left side of Figure 7), which is consistent with the asymptotic expression $1/\alpha^2$ of the Fisher information of the K-distribution [1] (corresponding to $k = 0$). Indeed, the larger the value of α, the smaller the information revealed by the data, so that a larger sample size is needed for a finer estimation. Henceforth, the limitation of the XU estimator for large values of α is intrinsic to the model. To further study this issue, we have experimented with simulated ultrasound images with 11 to 20 scatterers per resolution cell. The relative RMSEs for $1/\alpha$ were equal to 1.43 (MI), 1.27 (MA), 1.25 (XU), and 1.33 (RSK); for $1/(\kappa+1)$, we obtained 0.14 (MI), 0.16 (MA), 0.17 (XU), and 0.20 (RSK). Thus, the XU estimator is better than the other three for $1/\alpha$, but for $1/(\kappa+1)$, the MI estimator is best, whereas the XU estimator is still better than the RSK estimator.

One way to remedy this limitation is to consider the median of the estimator over a sequence of images. Figure 11 shows that this approach yields much better results for the parameter $1/(\kappa+1)$ and slightly better results for $1/\alpha$. Taking the median over all frames, instead of the mean, reduced the normalized bias[1] of the XU estimator for the parameter $1/(\kappa+1)$ to 0.08 in the case of the simulations with 11 to 20 diffuse scatterers. So, the bias

[1]The bias may be defined as $E[\hat{\theta}] - \theta$, where $\hat{\theta}$ is the parameter estimator and θ is the gold standard, or as median$(\hat{\theta}) - \theta$ when using the median instead of the mean.

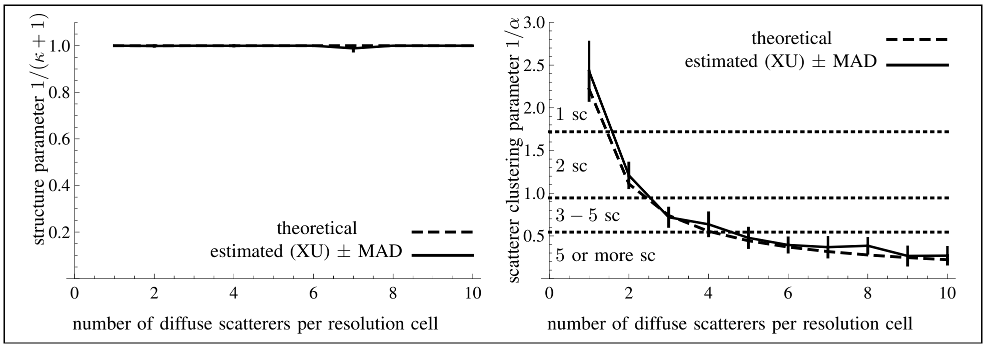

Figure 11. *Median values of the parameter* $1/(\kappa+1)$ *(left) and of the scatterer clustering parameter* $1/\alpha$ *(right) as a function of the average number of randomly located scatterers per resolution cell. No coherent component was included in these simulations. The sample size of each frame is* 13299*, and the number of frames is* $N = 60$ *(used for the computation of the median absolute deviations).*

was smaller when using the median instead of the mean. Moreover, the standard deviation (or the median absolute deviation (MAD) is proportional to $1/\sqrt{N}$ for the average of an estimator over N images. Thus, taking the median value of the estimator over a sequence of images greatly improves its performance.

Note also from Figure 11 that although the XU estimator does not allow the exact number of scatterers per resolution cell for $1/\alpha < 0.7$ to be distinguished, this estimator nevertheless indicates the range of the number of scatterers. This is consistent with the fact that the homodyned K-distribution gets close to a Rice distribution[2] as α increases, so that it becomes harder to determine the exact value of α. So, again, this phenomenon is intrinsic to the model.

5.2.2. Variation of the coherent component. As can be seen from Figure 10, the estimation of the parameter $1/(\kappa+1)$ is quite reliable except when the number of coherent scatterers is 1 or 2. Also, the estimated parameter $1/\alpha$ is smaller than the expected constant value in the case of the simulations with a variable coherent component. So, as it stands, the proposed theoretical model is only an approximation. For that reason, we have chosen two evaluation measures that do not depend on a theoretical ground-truth in Table 4 (right). For the parameter $1/\alpha$, the coefficient of variation (CV) of the estimated parameter indicates the variability of the estimator with respect to its mean. If $\hat{\theta}$ is the estimator of a parameter θ, the CV is defined as $\sqrt{Var[\hat{\theta}]}/E[\hat{\theta}]$. For the parameter $1/(\kappa+1)$, the root Fisher's J criterion (RFJC) applied to pairs of distinct values of the parameter is an indicator of the discrimination power of the estimator. For two distinct values of a parameter θ, say θ_1 and θ_2, the RFJC is defined as $|E[\hat{\theta_1}] - E[\hat{\theta_2}]|/\sqrt{Var[\hat{\theta_1}] + Var[\hat{\theta_2}]}$.

Table 4 (right) shows that the XU estimation method performed better than the other tested methods, even with RF SNRs of 20–5 dB. Note that, overall, the estimates improved

[2]We checked numerically that the Kullback–Leibler distance between a homodyned K-distribution with parameters ε, σ^2, α and the Rice distribution with parameters ε and $\sigma_{\mathrm{R}}^2 = \sigma^2\alpha$ is less than 8.8×10^{-3} for values in the range $k = \frac{\varepsilon}{\sigma\sqrt{\alpha}} \in \{0, 0.1, \ldots, 1.9, 2.0\}$ and $\alpha \in \{10, 11, \ldots, 20\}$. This represents a very good approximation. Note that the Kullback–Leibler distance is independent of the scaling factor μ so that one may assume that $\mu = 1$.

in the presence of less noise on the RF signal, as expected.

5.3. Computational load. In the case of the experiments of section 4.1, one estimation took on average 1.0 ms (MI), 1.6 ms (MA), 1.8 ms (XU), and 295.2 ms (RSK). In the case of the experiments of sections 4.2.2 and 4.2.3, the computation times per image were equal to 6.0 ms (MI), 8.0 ms (MA), 6.8 ms (XU), and 500 ms (RSK). So, the MI, MA, and XU methods share a comparable efficiency, whereas the RSK method is slower. That being said, the implementation for the first three methods was in C++, whereas the RSK method was implemented with MATLAB. Nevertheless, the first three methods resort to a binary search algorithm with a geometric rate of convergence, whereas the RSK method does not.

5.4. Hypothesis underlying the simulations of ultrasound images. As in [8, 11], we have made the hypothesis that the scatterers are dimensionless (upon using the Field II ultrasound simulation program [18, 17]). In the case of biological tissues, this hypothesis is false. In fact, the cell nuclei may be viewed as weak scatterers embedded in cytoplasm, considered as the ambient medium (see [34, 31]). Assuming spherical nuclei with a radius of 4.5 μm, one obtains a volume of 382 μm^3. For flowing red blood cells, which do not have a nucleus, the cells themselves are viewed as scatterers (of volume 94 μm^3 [32]), whereas the plasma is considered as the ambient medium. The point is that a sufficiently large density of scatterers with nonzero volume creates a scattering field that departs from the scattering behavior of uniformly distributed dimensionless scatterers, due to the so-called packing factor [36, 37]. Thus, the simulations reported in the present study are to be interpreted in the context of a low density of uniformly distributed weak scatterers of sufficiently small size (with respect to the resolution cell). The study of the homodyned K-distribution in the context of more realistic simulations with scatterers of finite dimensions would need to be addressed.

5.5. Conjecture 1. The statement that the algorithm of Figure 4 converges to a unique solution is proved in Appendix B. For the algorithm of Figure 5, all statements of Theorem 3.5 are proved in Appendix C. But Conjecture 1 remains to be proved to obtain the convergence of the algorithm of Figure 5 to a unique solution of the system of equations (3.1). Yet, we have explained in Appendix D how that conjecture would follow from two claims. The former claim is illustrated in Figure 12, whereas the latter is proved in Appendix D. We are convinced that the first claim is also true, but we do not know whether this strategy for proving the conjecture is the easiest one. Note that the algorithm of Figure 6 also relies on the conjecture.

5.6. Upper bound on the parameter α. If one does not impose an upper bound on α (unlike what was done in section 3.5), then one can consider the following minimization problem, which is similar to (3.8):

$$(\mu, \kappa, \beta) = \arg\min |U_{\text{HK}} - U| \quad \text{subject to } \mu = \overline{I} \text{ and } X_{\text{HK}} = X, \tag{5.1}$$

where $\kappa = \varepsilon^2/(2\sigma^2\alpha)$ and $\beta = 1/\alpha$. Observe that a solution to the system (3.1) automatically yields the solution $\mu = \bar{I}$, $\kappa = \varepsilon^2/(2\sigma^2\alpha) = \gamma/\alpha$, and $\beta = 1/\alpha$ to the system (5.1).

The first case where the conditions of Corollary 3.6 are not satisfied (i.e., when the system (3.1) has no solution) corresponds to $X > 1$ and $U_{\text{K}}(X_{\text{K}}^{-1}(X)) \geq U$. Since $U_{\text{K}}(X_{\text{K}}^{-1}(X))$ is the lower bound of the function $U_{\mathrm{HK}}(\gamma(\alpha, X), \alpha)$ (cf. Theorem 3.3), it follows that $|U_{\mathrm{HK}} - U|$ is minimized at $\alpha = \alpha_0 = 1/(X-1)$, assuming Conjecture 1. But then, one must have $\gamma(\alpha_0, X) = 0$, because of Theorem 3.3. Thus, one obtains the K-distribution model with $\mu = \bar{I}$, $\kappa = 0$, and $\alpha = \alpha_0$ (and hence $\beta = 1/\alpha_0$).

The other case to consider corresponds to $X \leq 1$ and $U_{\mathrm{Ri}}(X_{\mathrm{Ri}}^{-1}(X)) \geq U$. Then, $|U_{\mathrm{HK}} - U|$ is minimized at $\alpha = \infty$, assuming Conjecture 1. Indeed, the lower bound of the function $U_{\mathrm{HK}}(\gamma(\alpha, X), \alpha)$ is equal to $U_{\mathrm{Ri}}(X_{\mathrm{Ri}}^{-1}(X))$ and is reached asymptotically at infinity (cf. Theorem 3.5(c)). Thus, one obtains the Rice distribution. In fact, as $\alpha \to \infty$, the homodyned K-distribution with parameters ε^2, $\sigma^2 = \sigma_{\mathrm{R}}^2/\alpha$, and α tends to the Rice distribution with parameters ε^2 and σ_{R}^2. Moreover, from Appendix B, Proof of Theorem 3.5(c), we have $X_{\mathrm{Ri}}(\kappa) = \lim_{\alpha\to\infty} X_{\mathrm{HK}}(\gamma, \alpha)$, where $\kappa = \frac{\varepsilon^2}{2\sigma_{\mathrm{R}}^2}$ and $\gamma = \frac{\varepsilon^2}{2\sigma^2} = \frac{\varepsilon^2}{2\sigma_{\mathrm{R}}^2}\alpha = \kappa\alpha$. Furthermore, one obtains $\beta = \lim_{\alpha\to\infty} 1/\alpha = 0$. The special case where $X = 1$ yields the Rayleigh distribution because $X_{\mathrm{Ri}}(0) = 1$. Thus, if one is willing to include the Rice distribution to the homodyned K-distribution model as a limit case, then the system (5.1) always admits a solution.

However, the value of α is unbounded with that formulation, which is problematic in any implementation. For this reason, we adopted the minimization formulation of (3.8). Note that the MI and MA methods present a similar behavior. Moreover, the RSK method also restricts the parameters k and α to a bounded domain.

5.7. Biomedical applications.

The K-distribution was used in the context of breast cancer classification in [33]. The parameters of the K-distribution have also been studied in the context of tissue characterization under shear wave propagation [3]. The homodyned K-distribution was used for cardiac tissue characterization [10], cancerous lesion classification [25, 12, 22], breast lesion classification [35], and determination of red blood cell aggregation [7]. In all these applications, the statistical parameters of the distributions considered are viewed as classifying features. The underlying assumption is that the scattering properties of the biological tissues leave a signature on the echo envelope of the received RF signal.

6. Conclusions.

A method for the estimation of the parameters of the homodyned K-distribution was proposed, based on the first moment of the intensity and two log-moments (i.e., the U- and X-statistics). It was proved that the proposed algorithm converges to an estimation of the parameters. It was shown that it is preferable to estimate the parameters $1/(\kappa+1)$ and $1/\alpha$, rather than k or κ, and α. The experimental results reported here show that the resulting estimator is, overall, more reliable than the method [8] based on the first three intensity moments, or a method based on the first three moments of the amplitude, or the estimator [11] based on the SNR, the skewness, and the kurtosis of two fractional orders of the amplitude. These results hold even in the presence of noise corresponding to RF SNRs of 20–5 dB. For simulated data samples, the method [11] was slightly better for the parameter $1/(\kappa+1)$. For simulated ultrasound images with more than 10 scatterers per resolution cell, the estimator [8] was slightly better for the parameter $1/(\kappa+1)$. Otherwise, the proposed estimator ranked best among the four tested estimation methods. Moreover, the proposed method has a geometric rate of convergence, since it is based on the bisection algorithm for monotonous functions. Thus, a fast, reliable, and novel algorithm for the estimation of the homodyned K-distribution was proposed. On theoretical grounds, the uniqueness of the solution produced by the proposed method remains to be proved.

Appendix A. The statistics U and X for the homodyned K-distribution. In this appendix and those which follow, the software Mathematica (Wolfram Research, Inc., Champaign, IL, version 7.0) was used whenever possible for the computations of integrals or limits. We have indicated any step that could not be obtained directly from that software.

Proof of Lemma 3.1. Part (a). The function $\log I$ is concave. Therefore, from Jensen's inequality [16], one obtains $E[\log I] < \log E[I]$, since the random variable I is nonconstant.

Part (b). The function $I \log I$ is convex. Thus, $E[I \log I] > E[I] \log E[I]$. From part (a), one concludes that $E[I \log I] > E[I]E[\log I]$. ■

Proof of Proposition 3.2. Part (a). First, using the change of variable $I = A^2$, one computes

$$\int_0^\infty \log A^2 P_{\mathrm{Ri}}(A \mid \varepsilon, a^2)\, dA = \int_0^\infty \log I \frac{1}{2a^2} I_0\Big(\frac{\varepsilon}{a^2}\sqrt{I}\Big) e^{-\varepsilon^2/(2a^2)} e^{-I/(2a^2)}\, dI, \tag{A.1}$$

which is a Laplace transform equal to $\Gamma(0, \frac{\varepsilon^2}{2a^2}) + \log \varepsilon^2$, where $\Gamma(0, x)$ is the incomplete gamma function $\int_x^\infty \frac{e^{-t}}{t}\, dt$. Then, taking $a^2 = \sigma^2 w$, multiplying by $\mathcal{G}(w \mid \alpha, 1)$, and integrating with respect to w, one obtains

$$\begin{aligned} &-\gamma_E + \log(2\sigma^2) + \psi(\alpha) \\ &- \left(\frac{\varepsilon^2}{2\sigma^2}\right)^\alpha \frac{\Gamma(-\alpha)}{\alpha\Gamma(\alpha)}\, {}_1F_2\left(\alpha; 1+\alpha, 1+\alpha; \frac{\varepsilon^2}{2\sigma^2}\right) + \frac{\varepsilon^2}{2\sigma^2} \frac{\Gamma(\alpha-1)}{\Gamma(\alpha)}\, {}_2F_3\left(1, 1; 2, 2, 2-\alpha; \frac{\varepsilon^2}{2\sigma^2}\right). \end{aligned} \tag{A.2}$$

Subtracting $\log E[I]$ from (A.2), with the identity $E[I] = \varepsilon^2 + 2\sigma^2\alpha$, and setting $\gamma = \varepsilon^2/(2\sigma^2)$ yields the result.

Part (b). Again, using the change of variable $I = A^2$, one computes

$$\int_0^\infty A^2 \log A^2 P_{\mathrm{Ri}}(A \mid \varepsilon, a^2)\, dA = \int_0^\infty I \log I \frac{1}{2a^2} I_0\Big(\frac{\varepsilon}{a^2}\sqrt{I}\Big) e^{-\varepsilon^2/(2a^2)} e^{-I/(2a^2)}\, dI. \tag{A.3}$$

This Laplace transform is equal to $4a^2 - 2e^{-\frac{\varepsilon^2}{2a^2}} a^2 + (\varepsilon^2 + 2a^2)(\Gamma(0, \frac{\varepsilon^2}{2a^2}) + \log \varepsilon^2)$. Then, subtracting by $(\varepsilon^2 + 2\sigma^2\alpha) \int_0^\infty \log A^2 P_{\mathrm{Ri}}(A \mid \varepsilon, a^2)\, dA$ (corresponding to the term $-E[I]E[\log I]$), taking $a^2 = \sigma^2 w$, and multiplying by $\mathcal{G}(w \mid \alpha, 1)$, one obtains

$$\begin{aligned} &2\sigma^2 w\big(-e^{-\frac{\varepsilon^2}{2\sigma^2 w}} + 2\big)\mathcal{G}(w, \alpha) + 2\sigma^2 \Gamma\left(0, \frac{\varepsilon^2}{2\sigma^2 w}\right)\big(-\alpha + w\big)\mathcal{G}(w, \alpha) \\ &+ 2\sigma^2 \log \varepsilon^2 \big(-\alpha + w\big)\mathcal{G}(w, \alpha). \end{aligned} \tag{A.4}$$

Then, integrating with respect to w yields

$$\begin{aligned} &2\sigma^2 + 4\sigma^2\alpha - \frac{2^{3/2}\varepsilon\sigma}{\Gamma(\alpha)} \left(\frac{\varepsilon^2}{2\sigma^2}\right)^{\alpha/2} K_{\alpha+1}\left(\frac{\sqrt{2}\varepsilon}{\sigma}\right) \\ &+ 2\sigma^2 \frac{\Gamma(-\alpha)}{\Gamma(\alpha)} \left(\frac{\varepsilon^2}{2\sigma^2}\right)^\alpha {}_1F_2\left(\alpha; 1+\alpha, 1+\alpha; \frac{\varepsilon^2}{2\sigma^2}\right) \\ &- \varepsilon^2 \frac{\Gamma(-1-\alpha)}{(1+\alpha)\Gamma(\alpha)} \left(\frac{\varepsilon^2}{2\sigma^2}\right)^\alpha {}_1F_2\left(1+\alpha; 2+\alpha, 2+\alpha; \frac{\varepsilon^2}{2\sigma^2}\right) \\ &+ \varepsilon^2\, {}_2F_3\left(1, 1; 2, 2, 1-\alpha; \frac{\varepsilon^2}{2\sigma^2}\right) - \varepsilon^2 \frac{\alpha\Gamma(-1+\alpha)}{\Gamma(\alpha)}\, {}_2F_3\left(1, 1; 2, 2, 2-\alpha; \frac{\varepsilon^2}{2\sigma^2}\right), \end{aligned} \tag{A.5}$$

which gives an expression for $E[I \log I] - E[I]E[\log I]$. Dividing (A.5) by $E[I] = \varepsilon^2 + 2\sigma^2\alpha$ and setting $\gamma = \varepsilon^2/(2\sigma^2)$ yields the result. ■

Appendix B. Estimating γ when α is known.

Proof of Theorem 3.3. Part (a). By definition of the hypergeometric series as a power series, one has ${}_pF_q(a_1, \dots, a_p; b_1, \dots, b_q; x) = 1$ at $x = 0$. Using this fact, one concludes that the sum of the last four terms in (3.4) is equal to 0 at $\gamma = 0$. Next, from [2, eq. (9.6.9), p. 375], one has the asymptotic behavior $K_\alpha(x) \sim \frac{\Gamma(\alpha)}{2}\left(\frac{2}{x}\right)^\alpha$ at $x = 0$. Hence, the second term of (3.4) admits the asymptotic form $-\frac{2\gamma^{\alpha/2+1/2}}{(\gamma+\alpha)\Gamma(\alpha)}\frac{\Gamma(\alpha+1)}{2}\left(\frac{1}{\gamma^{1/2}}\right)^{\alpha+1} = -\frac{\alpha}{(\gamma+\alpha)} = -1$ at $\gamma = 0$. Collecting all terms, one obtains $\lim_{\gamma\to 0} \frac{1+2\alpha}{(\gamma+\alpha)} - \frac{\alpha}{(\gamma+\alpha)} = 1 + \frac{1}{\alpha}$. Since $\gamma = 0$ corresponds to the K-distribution, this also shows that $X_{\mathrm{K}}(\alpha) = 1 + 1/\alpha$.

Part (b). Writing (A.4) in terms of γ and α, and dividing by $\mu = E[I]$, one obtains

$$\text{(B.1)} \qquad \begin{aligned} &\frac{w}{(\gamma+\alpha)}\left(-e^{-\frac{\gamma}{w}} + 2\right)\mathcal{G}(w,\alpha) + \frac{\Gamma(0,\frac{\gamma}{w})}{(\gamma+\alpha)}(-\alpha+w)\mathcal{G}(w,\alpha) \\ &+ \frac{\log\varepsilon^2}{(\gamma+\alpha)}(-\alpha+w)\mathcal{G}(w,\alpha). \end{aligned}$$

The third term of (B.1) is irrelevant because its integral with respect to w is equal to 0. Thus, one has

$$\text{(B.2)} \qquad \begin{aligned} X_{\mathrm{HK}}(\gamma,\alpha) &= \int_0^\infty F(w,\gamma,\alpha)\,dw, \\ F(w,\gamma,\alpha) &= \frac{w}{(\gamma+\alpha)}\left(-e^{-\frac{\gamma}{w}} + 2\right)\mathcal{G}(w,\alpha) + \frac{\Gamma(0,\frac{\gamma}{w})}{(\gamma+\alpha)}(-\alpha+w)\mathcal{G}(w,\alpha). \end{aligned}$$

Claim 1. $|\Gamma(0, 1/x)| = \Gamma(0, 1/x) \le \sqrt{x}$ *for any* $x > 0$.

Proof. Let $f(x) = \Gamma(0, 1/x) - \sqrt{x}$. On the one hand, $\lim_{x\to 0} f(x) = 0$. On the other hand, $\frac{d}{dx}f(x) = \frac{e^{-1/x}}{x} - \frac{1}{2\sqrt{x}} < 0$ for $x > 0$. This last statement is equivalent to $2/\sqrt{x} < e^{1/x}$ for $x > 0$ or $4z < e^{2z}$ for $z > 0$ (with the change of variable $z = 1/x$). But now, the function $g(z) = e^{2z} - 4z$ has an absolute minimum at $z_0 = \frac{1}{2}\log 2$ (because $\frac{d}{dz}g(z) < 0$ for $z < z_0$, whereas $\frac{d}{dz}g(z) > 0$ for $z > z_0$), and furthermore, $g(z_0) = 2(1 - \log 2) > 0$. So, $g(z) > 0$ for all $z > 0$, which completes the proof of the claim. ■

From the claim, $|\Gamma(0, \frac{\gamma}{w})| \le \sqrt{\frac{w}{\gamma}}$. Therefore, the absolute value of the function $F(w,\gamma,\alpha)$ of (B.2) admits the upper bound

$$\text{(B.3)} \qquad \frac{2w}{(\gamma+\alpha)}\mathcal{G}(w,\alpha) + \frac{w^{1/2}}{\gamma^{1/2}(\gamma+\alpha)}(\alpha+w)\mathcal{G}(w,\alpha).$$

Integrating (B.3) with respect to w yields $\frac{2\alpha}{(\gamma+\alpha)} + \frac{(1+4\alpha)\Gamma(1/2+\alpha)}{2\gamma^{1/2}(\gamma+\alpha)\Gamma(\alpha)}$. Thus, $\lim_{\gamma\to\infty} X_{\mathrm{HK}}(\gamma,\alpha) = 0$.

Part (c). From (B.2), the function $X_{\mathrm{HK}}(\gamma,\alpha)$ can be written as the sum of the following two functions:

$$X_{\mathrm{HK},A}(\gamma,\alpha) = \int_0^\infty \frac{w}{(\gamma+\alpha)}(-e^{-\frac{\gamma}{w}}+2)\mathcal{G}(w,\alpha)\,dw,$$
$$X_{\mathrm{HK},B}(\gamma,\alpha) = \int_0^\infty \frac{\Gamma(0,\frac{\gamma}{w})}{(\gamma+\alpha)}(-\alpha+w)\mathcal{G}(w,\alpha)\,dw. \tag{B.4}$$

It is now shown that the first function is decreasing in γ and that the second one is strictly decreasing in γ.

First, one computes

$$\begin{aligned}\frac{\partial}{\partial\gamma}X_{\mathrm{HK},A}(\gamma,\alpha) &= \int_0^\infty \left\{\frac{1}{(\gamma+\alpha)}e^{-\frac{\gamma}{w}} + \frac{w}{(\gamma+\alpha)^2}\Big(e^{-\frac{\gamma}{w}}-2\Big)\right\}\mathcal{G}(w,\alpha)\,dw \\ &\le \int_0^\infty \left\{\frac{1}{(\gamma+\alpha)}\frac{1}{(1+\gamma/w)} + \frac{w}{(\gamma+\alpha)^2}\left(\frac{1}{(1+\gamma/w)}-2\right)\right\}\mathcal{G}(w,\alpha)\,dw \\ &= \frac{\alpha}{(\gamma+\alpha)^2}\Big(-1+e^{\gamma}\,\alpha\,E(1+\alpha,\gamma)\Big),\end{aligned} \tag{B.5}$$

where $E(1+\alpha,\gamma)=\int_1^\infty e^{-\gamma t}t^{-\alpha-1}\,dt$. So, one concludes that $\frac{\partial}{\partial\gamma}X_{\mathrm{HK},A}(\gamma,\alpha)\le 0$ from Claim 2 below.

Claim 2. *For $\gamma>0$ and $\alpha>0$, $E(1+\alpha,\gamma)\le e^{-\gamma}/\alpha$.*

Proof. Since $e^{-\gamma t}\le e^{-\gamma}$ for $t\ge 1$ and $t^{-\alpha-1}>0$, one immediately computes the inequality $\int_1^\infty e^{-\gamma t}t^{-\alpha-1}\,dt \le e^{-\gamma}\int_1^\infty t^{-\alpha-1}\,dt = e^{-\gamma}/\alpha$. ■

Next, one may write $X_{\mathrm{HK},B}(\gamma,\alpha)$ as $\frac{1}{(\gamma+\alpha)}X_{\mathrm{HK},C}(\gamma,\alpha)$, where

$$X_{\mathrm{HK},C}(\gamma,\alpha) = \int_0^\infty \Gamma\left(0,\frac{\gamma}{w}\right)(-\alpha+w)\mathcal{G}(w,\alpha)\,dw. \tag{B.6}$$

Hence, $\frac{\partial}{\partial\gamma}X_{\mathrm{HK},B}(\gamma,\alpha) = -\frac{1}{(\gamma+\alpha)^2}X_{\mathrm{HK},C}(\gamma,\alpha)+\frac{1}{(\gamma+\alpha)}\frac{\partial}{\partial\gamma}X_{\mathrm{HK},C}(\gamma,\alpha)$. Thus, in order to show that $X_{\mathrm{HK},B}$ is strictly decreasing, it is sufficient to show that $X_{\mathrm{HK},C}(\gamma,\alpha)>0$ and that $X_{\mathrm{HK},C}(\gamma,\alpha)$ is decreasing. Therefore, it is sufficient to prove Claims 3 and 4 below.

Claim 3. *For $\gamma>0$ and $\alpha>0$, $\frac{\partial}{\partial\gamma}X_{\mathrm{HK},C}(\gamma,\alpha)<0$.*

Proof. One computes

$$\frac{\partial}{\partial\gamma}X_{\mathrm{HK},C}(\gamma,\alpha) = \int_0^\infty -\frac{e^{-\frac{\gamma}{w}}}{\gamma}(-\alpha+w)\mathcal{G}(w,\alpha)\,dw = -\frac{2\gamma^{(\alpha-1)/2}}{\Gamma(\alpha)}K_{\alpha-1}(2\sqrt{\gamma})<0. \qquad ■$$

Claim 4. *For $\alpha>0$, $\lim_{\gamma\to\infty}X_{\mathrm{HK},C}(\gamma,\alpha)=0$.*

Proof. Observe that $|\Gamma(0,1/x)|=\Gamma(0,1/x)\le x$ for $x>0$. Indeed, let $f(x)=\Gamma(0,1/x)-x$. Then, $\lim_{x\to0}f(x)=0$, and $\frac{d}{dx}f(x)=\frac{e^{-1/x}}{x}-1<0$, because $e^{1/x}>1/x$ for $x>0$. Hence, one has $|X_{\mathrm{HK},C}(\gamma,\alpha)|\le\int_0^\infty\frac{w}{\gamma}(\alpha+w)\mathcal{G}(w,\alpha)\,dw=\frac{\alpha(1+2\alpha)}{\gamma}$. But, $\lim_{\gamma\to\infty}\frac{\alpha(1+2\alpha)}{\gamma}=0$. ■

This completes the proof of the theorem. ■

Appendix C. Estimating γ and α.

Lemma C.1.
(a) $\lim_{\alpha\to 0} X_{\mathrm{HK}}(\alpha/x,\alpha) = \infty$ *for any* $x > 0$.
(b) $\lim_{\alpha\to 0} U_{\mathrm{HK}}(\alpha/x,\alpha) = -\log(1+x)$ *for any* $x > 0$.

Proof. Part (a). Setting $\gamma = \alpha/x$, (3.4) reads as

$$\begin{aligned}
X_{\mathrm{HK}}(\alpha/x,\alpha) &= \frac{1}{(1/x+1)}\frac{(1+2\alpha)}{\alpha} \\
&- \frac{2}{x^{\alpha/2+1/2}(1/x+1)}\frac{\alpha^{\alpha/2-1/2}}{\Gamma(\alpha)}K_{\alpha+1}\Big(2\sqrt{\alpha/x}\Big) \\
&+ \frac{1}{x^{\alpha}(1/x+1)}\frac{\Gamma(-\alpha)\alpha^{\alpha-1}}{\Gamma(\alpha)}\,{}_1F_2\Big(\alpha;1+\alpha,1+\alpha;\frac{\alpha}{x}\Big) \\
&- \frac{1}{x^{\alpha+1}(1/x+1)}\frac{\Gamma(-1-\alpha)\alpha^{\alpha}}{(1+\alpha)\Gamma(\alpha)}\,{}_1F_2\Big(1+\alpha;2+\alpha,2+\alpha;\frac{\alpha}{x}\Big) \\
&+ \frac{1}{(x+1)}\,{}_2F_3\Big(1,1;2,2,1-\alpha;\frac{\alpha}{x}\Big) - \frac{1}{(x+1)}\frac{\alpha\Gamma(-1+\alpha)}{\Gamma(\alpha)}\,{}_2F_3\Big(1,1;2,2,2-\alpha;\frac{\alpha}{x}\Big).
\end{aligned} \tag{C.1}$$

Using the definition of the hypergeometric series, one sees immediately that $1 \le {}_1F_2(\alpha;1+\alpha,1+\alpha;\alpha/x) \le {}_1F_2(1/2;1,1;\alpha/x)$ for $\alpha \le 1/2$; moreover, $\lim_{\alpha\to 0}\frac{\Gamma(-\alpha)\alpha^{\alpha-1}}{\Gamma(\alpha)} = -\infty$. Therefore, $\frac{\Gamma(-\alpha)\alpha^{\alpha-1}}{\Gamma(\alpha)}\,{}_1F_2(\alpha;1+\alpha,1+\alpha;\alpha/x) \ge \frac{\Gamma(-\alpha)\alpha^{\alpha-1}}{\Gamma(\alpha)}\,{}_1F_2(1/2;1,1;\alpha/x)$ for α sufficiently small. Now, ${}_1F_2(1/2;1,1;\alpha/x)$ is a power series in the variable α; moreover, $\lim_{\alpha\to 0}\frac{\Gamma(-\alpha)\alpha^{\alpha-1}}{\Gamma(\alpha)}\alpha = -1$ and $\lim_{\alpha\to 0}\frac{\Gamma(-\alpha)\alpha^{\alpha-1}}{\Gamma(\alpha)}\alpha^n = 0$ for $n > 1$. Therefore, $\frac{\Gamma(-\alpha)\alpha^{\alpha-1}}{\Gamma(\alpha)}\,{}_1F_2(\alpha;1+\alpha,1+\alpha;\alpha/x) \ge \frac{\Gamma(-\alpha)\alpha^{\alpha-1}}{\Gamma(\alpha)} + \textit{constant}$ for α sufficiently small. Arguing as above, $\lim_{\alpha\to 0}{}_1F_2(1+\alpha;2+\alpha,2+\alpha;\alpha/x) = 1$. In the same manner, one sees that $1 \le {}_2F_3(1,1;2,2,1-\alpha;\alpha/x) \le {}_2F_3(1,1;2,2,1/2;\alpha/x)$ for $\alpha \le 1/2$, but, one has that $\lim_{\alpha\to 0}{}_2F_3(1,1;2,2,1/2;\alpha/x) = 1$. Similarly, one shows that $\lim_{\alpha\to 0}{}_2F_3(1,1;2,2,2-\alpha;\alpha/x) = 1$. From there, one obtains

$$\begin{aligned}
&\frac{\Gamma(-\alpha)\alpha^{\alpha-1}}{\Gamma(\alpha)}\,{}_1F_2(\alpha;1+\alpha,1+\alpha;\alpha/x) \ge \frac{\Gamma(-\alpha)\alpha^{\alpha-1}}{\Gamma(\alpha)} + \textit{constant}, \\
&\lim_{\alpha\to 0} -\frac{\Gamma(-1-\alpha)\alpha^{\alpha}}{(1+\alpha)\Gamma(\alpha)}\,{}_1F_2(1+\alpha;2+\alpha,2+\alpha;\alpha/x) = -1, \\
&\lim_{\alpha\to 0}{}_2F_3(1,1;2,2,1-\alpha;\alpha/x) = 1, \\
&\lim_{\alpha\to 0} -\frac{\alpha\Gamma(-1+\alpha)}{\Gamma(\alpha)}\,{}_2F_3(1,1;2,2,2-\alpha;\alpha/x) = 0\times 1.
\end{aligned} \tag{C.2}$$

Using the limiting form $K_1(z) \sim z^{-1}$ [2, eq. (9.6.9), p. 375] valid for small arguments z, one computes

$$\lim_{\alpha\to 0} -\frac{\alpha^{\alpha/2-1/2}}{\Gamma(\alpha)}K_{\alpha+1}\left(2\sqrt{\frac{\alpha}{x}}\right) = -\frac{\sqrt{x}}{2}. \tag{C.3}$$

Finally, combining equations (C.1), (C.2), and (C.3), one has $\liminf_{\alpha\to 0} X_{\mathrm{HK}}(\alpha/x,\alpha) \ge \liminf_{\alpha\to 0}\frac{1}{(1/x+1)}\frac{(1+2\alpha)}{\alpha} + \frac{1}{x^{\alpha}(1/x+1)}\frac{\Gamma(-\alpha)\alpha^{\alpha-1}}{\Gamma(\alpha)} + \textit{constant} = \infty$.

Part (b). Setting $\gamma = \alpha/x$, (3.3) reads as

$$-\gamma_E - \log\left(\frac{\alpha}{x}+\alpha\right) + \psi(\alpha) - \left(\frac{\alpha}{x}\right)^{\alpha}\frac{\Gamma(-\alpha)}{\alpha\Gamma(\alpha)}\,{}_1F_2\left(\alpha;1+\alpha,1+\alpha;\frac{\alpha}{x}\right) + \left(\frac{\alpha}{x}\right)\frac{\Gamma(\alpha-1)}{\Gamma(\alpha)}\,{}_2F_3\left(1,1;2,2,2-\alpha;\frac{\alpha}{x}\right). \tag{C.4}$$

Using the definition of the hypergeometric series, one sees immediately that $1 \le {}_2F_3(1,1;2,2,2-\alpha;\alpha/x) \le {}_2F_3(1,1;2,2,3/2;\alpha/x)$ for $\alpha \le 1/2$, but, on the other hand, one has $\lim_{\alpha\to 0} {}_2F_3(1,1;2,2,3/2;\alpha/x) = 1$. So, $\lim_{\alpha\to 0} {}_2F_3(1,1;2,2,2-\alpha;\alpha/x) = 1$. Since $\lim_{\alpha\to 0}(\alpha/x)\frac{\Gamma(\alpha-1)}{\Gamma(\alpha)} = 0$, one concludes that $\lim_{\alpha\to 0}(\alpha/x)\frac{\Gamma(\alpha-1)}{\Gamma(\alpha)} \times {}_2F_3(1,1;2,2,2-\alpha;\alpha/x) = 0$. Next, one writes ${}_1F_2(\alpha;1+\alpha,1+\alpha;\alpha/x) = 1 + h(x,\alpha)$, where $h(x,\alpha) = \sum_{n=1}^{\infty}\frac{(\alpha)_n}{(1+\alpha)_n(1+\alpha)_n}\frac{(\alpha/x)^n}{n!}$. Let us observe that $0 \le h(x,\alpha) \le \sum_{n=1}^{\infty}\alpha\,(\alpha/x)^n = \frac{\alpha^2}{x}\frac{1}{1-\alpha/x}$ (for α sufficiently small), and from there it follows that $\lim_{\alpha\to 0}(\alpha/x)^{\alpha}\frac{\Gamma(-\alpha)}{\alpha\Gamma(\alpha)}h(x,\alpha) = 0$. Finally, one has $\lim_{\alpha\to 0} -\gamma_E - \log(\alpha/x + \alpha) + \psi(\alpha) - (\alpha/x)^{\alpha}\frac{\Gamma(-\alpha)}{\alpha\Gamma(\alpha)} = -\log(1+x)$. ■

Lemma C.2. *For any $\gamma > 0$ and $\alpha > 0$, $\frac{\partial}{\partial\gamma}U_{\mathrm{HK}}(\gamma,\alpha) > 0$.*

Proof. From the proof of Proposition 3.2(a), one has

$$U_{\mathrm{HK}}(\gamma,\alpha) = \int_0^{\infty}\left(\Gamma\left(0,\frac{\gamma}{w}\right) + \log\frac{\gamma}{\gamma+\alpha}\right)\mathcal{G}(w\mid\alpha,1)\,dw. \tag{C.5}$$

So, one computes

$$\begin{aligned}\frac{\partial}{\partial\gamma}U_{\mathrm{HK}}(\gamma,\alpha) &= \int_0^{\infty}\frac{\partial}{\partial\gamma}\left(\Gamma\left(0,\frac{\gamma}{w}\right) + \log\frac{\gamma}{\gamma+\alpha}\right)\mathcal{G}(w\mid\alpha,1)\,dw \\ &= \int_0^{\infty}\frac{1}{\gamma}\left(-e^{-\frac{\gamma}{w}} + \frac{\alpha}{(\gamma+\alpha)}\right)\mathcal{G}(w\mid\alpha,1)\,dw \\ &\ge \int_0^{\infty}\frac{1}{\gamma}\left(-\frac{1}{(1+\gamma/w)} + \frac{\alpha}{(\gamma+\alpha)}\right)\mathcal{G}(w\mid\alpha,1)\,dw \\ &= \frac{e^{\gamma}\,\alpha}{(\gamma+\alpha)}\Big(E(\alpha,\gamma) - E(\alpha+1,\gamma)\Big),\end{aligned} \tag{C.6}$$

where $E(\alpha,\gamma) = \int_1^{\infty} e^{-\gamma t}t^{-\alpha}\,dt$. Since the function $E(\alpha,\gamma)$ is obviously decreasing in the variable α for a fixed value of γ, the result follows. ■

Proof of Theorem 3.5. Part (a). Let $x > 0$ be fixed for now. From Lemma C.1(a) and Theorem 3.3(c), one has that $\gamma(\alpha,X) > \alpha/x$ for α sufficiently small. Then, from Lemma C.2, one obtains that $U_{\mathrm{HK}}(\alpha/x,\alpha) < U_{\mathrm{HK}}(\gamma(\alpha,X),\alpha) < 0$ for α sufficiently small. Therefore, using Lemma C.1(b), one has $-\log(1+x) = \lim_{\alpha\to 0} U_{\mathrm{HK}}(\alpha/x,\alpha) \le \limsup_{\alpha\to 0} U_{\mathrm{HK}}(\gamma(\alpha,X),\alpha) \le 0$. Since $x > 0$ can be taken arbitrarily small, one deduces that $\lim_{\alpha\to 0} U_{\mathrm{HK}}(\gamma(\alpha,X),\alpha) = 0$.

Part (b). Let $X > 1$. From Theorem 3.3, one has that $\alpha = X_{\mathrm{K}}^{-1}(X) = 1/(X-1)$ implies that $\gamma(\alpha,X) = 0$. Then, taking $\gamma = 0$ and $\alpha = X_{\mathrm{K}}^{-1}(X)$ in (3.3) yields the result.

Part (c). Let $X \le 1$. The homodyned K-distribution with parameters ε^2, $\sigma^2 = \sigma_{\mathrm{R}}^2/\alpha$, α tends to the Rice distribution with parameters ε^2 and σ_{R}^2 as $\alpha \to \infty$. The structure parameter

κ for that Rice distribution is equal to $\frac{\varepsilon^2}{2\sigma_{\mathrm{R}}^2}$, and this is the same value for the homodyned K-distribution (because $2\sigma^2\alpha = 2(\sigma_{\mathrm{R}}^2/\alpha)\,\alpha = 2\sigma_{\mathrm{R}}^2$). Therefore, $\lim_{\alpha\to\infty} X_{\mathrm{HK}}(\kappa\alpha,\alpha) = X_{\mathrm{Ri}}(\kappa)$, since $\gamma = \kappa\alpha$. In the same manner, one obtains $\lim_{\alpha\to\infty} U_{\mathrm{HK}}(\kappa\alpha,\alpha) = U_{\mathrm{Ri}}(\kappa)$. Now, take $\kappa = X_{\mathrm{Ri}}^{-1}(X)$ and let $0<\eta<\kappa$. Then, for α sufficiently large, one has $(\kappa-\eta)\alpha < \gamma(\alpha,X) < (\kappa+\eta)\alpha$. Therefore, one obtains $U_{\mathrm{HK}}((\kappa-\eta)\alpha,\alpha) < U_{\mathrm{HK}}(\gamma(\alpha,X),\alpha) < U_{\mathrm{HK}}((\kappa+\eta)\alpha,\alpha)$, since from Lemma C.2, the function $U_{\mathrm{HK}}(\gamma,\alpha)$ is increasing in the variable γ. Taking the limit as $\alpha\to\infty$ (which is possible since $0<X\le 1$ implies that $\gamma(\alpha,X)$ is well defined for any $\alpha>0$), one deduces that $U_{\mathrm{Ri}}(\kappa-\eta) \le \liminf_{\alpha\to\infty} U_{\mathrm{HK}}(\gamma(\alpha,X),\alpha) \le \limsup_{\alpha\to\infty} U_{\mathrm{HK}}(\gamma(\alpha,X),\alpha) \le U_{\mathrm{Ri}}(\kappa+\eta)$. Since $\eta>0$ can be taken arbitrarily small, the result follows.

Next, an argument similar to the proof of Theorem 3.3 (i.e., making the change of variable $I = A^2$ and computing Laplace transforms) shows that $U_{\mathrm{Ri}}(\kappa) = \Gamma(0,\kappa) + \log\frac{\kappa}{(\kappa+1)}$ and $X_{\mathrm{Ri}}(\kappa) = \frac{(2-e^{-\kappa})}{(\kappa+1)}$. Finally, from basic calculus, one obtains the statement on the function $X_{\mathrm{Ri}}(\kappa)$. ■

Appendix D. Discussion on Conjecture 1. Let $f(\alpha) = U_{\mathrm{HK}}(\gamma(\alpha,X),\alpha)$ (X being known). Then, Conjecture 1 amounts to the inequality

$$\text{(D.1)}\qquad \frac{d}{d\alpha}f(\alpha) = \frac{\partial}{\partial\gamma}U_{\mathrm{HK}}(\gamma,\alpha)\frac{\partial}{\partial\alpha}\gamma(\alpha,X) + \frac{\partial}{\partial\alpha}U_{\mathrm{HK}}(\gamma,\alpha) < 0,$$

where $\gamma=\gamma(\alpha,X)$. Since $\gamma(\alpha,X)$ is defined by the identity $X_{\mathrm{HK}}(\gamma(\alpha,X),\alpha)\equiv X$, the implicit function theorem implies that $\frac{\partial}{\partial\alpha}\gamma(\alpha,X) = -\frac{\frac{\partial}{\partial\alpha}X_{\mathrm{HK}}(\gamma,\alpha)}{\frac{\partial}{\partial\gamma}X_{\mathrm{HK}}(\gamma,\alpha)}$. Moreover, since $\frac{\partial}{\partial\gamma}X_{\mathrm{HK}}(\gamma,\alpha)<0$, we conclude that (D.1) is equivalent to

$$\text{(D.2)}\qquad \Delta(\gamma,\alpha) = \frac{\partial}{\partial\gamma}X_{\mathrm{HK}}(\gamma,\alpha)\frac{\partial}{\partial\alpha}U_{\mathrm{HK}}(\gamma,\alpha) - \frac{\partial}{\partial\alpha}X_{\mathrm{HK}}(\gamma,\alpha)\frac{\partial}{\partial\gamma}U_{\mathrm{HK}}(\gamma,\alpha) > 0.$$

In particular, it is sufficient to prove the inequality $\Delta(\gamma,\alpha)>0$ for any $\gamma>0$ and $\alpha>0$. For this purpose, it is sufficient to show the following two claims.

Claim 5. *For any fixed value of $x>0$, the function $\Delta(\alpha x,\alpha)$ is decreasing in the variable $\alpha>0$.*

We have not succeeded in proving Claim 5, but Figure 12 convinced us that it is true.

Claim 6. *For any fixed value of $x>0$, $\lim_{\alpha\to\infty}\Delta(\alpha x,\alpha)=0$.*

Proof. Using the identity $\gamma = x\alpha$ and making the change of variable $w=\alpha w'$, we obtain from (C.6)

$$\text{(D.3)}\qquad \begin{aligned}\frac{\partial}{\partial\gamma}U_{\mathrm{HK}}(x\alpha,\alpha) &= \int_0^\infty \frac{1}{\gamma}\left(-e^{-\frac{\gamma}{w}} + \frac{\alpha}{(\gamma+\alpha)}\right)\mathcal{G}(w\mid\alpha,1)\,dw\\ &= \frac{1}{\alpha}\int_0^\infty \frac{1}{x}\left(-e^{-\frac{x}{w'}} + \frac{1}{(x+1)}\right)\mathcal{G}(w'\mid\alpha,1/\alpha)\,dw'.\end{aligned}$$

The distribution $\mathcal{G}(w'|\alpha,1/\alpha)$ is concentrated on $w'=1$ as $\alpha\to\infty$. Therefore, $\frac{\partial}{\partial\gamma}U_{\mathrm{HK}}(x\alpha,\alpha)\sim$

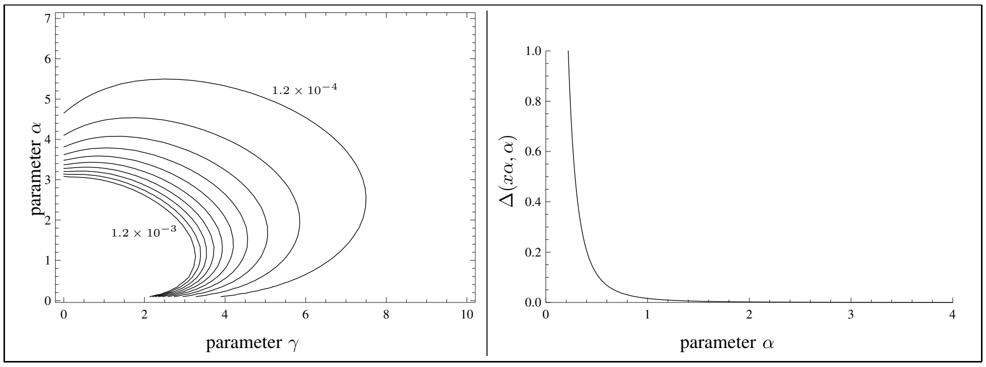

Figure 12. *Left: A few level curves of the function $\Delta(\gamma, \alpha)$ by steps of 1.2×10^{-4}. The function Δ is increasing in the direction pointing to the origin. Right: Typical graph of $\Delta(x\alpha, \alpha)$ for a fixed value of x.*

$\frac{1}{\alpha}\frac{1}{x}\{-e^{-\frac{x}{w'}} + \frac{1}{(x+1)}\}\big|_{w'=1} = \frac{O(1)}{\alpha}$ for large values of α. Similarly, we have

(D.4)
$$\frac{\partial}{\partial\alpha}U_{\mathrm{HK}}(x\alpha, \alpha) = \int_0^\infty \Gamma\left(0, \frac{\gamma}{w}\right)\left(\log w - \psi(\alpha)\right)\mathcal{G}(w \mid \alpha, 1)\, dw - \frac{1}{(\gamma+\alpha)}$$
$$= \int_0^\infty \Gamma\left(0, \frac{x}{w'}\right)\left(\log w' + \log\alpha - \psi(\alpha)\right)\mathcal{G}\left(w' \mid \alpha, \frac{1}{\alpha}\right) dw' - \frac{1}{\alpha(x+1)}.$$

Thus, $\frac{\partial}{\partial\alpha}U_{\mathrm{HK}}(x\alpha, \alpha) = O(1) + \Gamma(0, x)(\log\alpha - \psi(\alpha)) + \frac{O(1)}{\alpha} = O(1) + O(1)(\log\alpha - \psi(\alpha))$ for large values of α.

Next, we have for the X-statistics

$$\frac{\partial}{\partial\gamma}X_{\mathrm{HK}}(x\alpha, \alpha) = \int_0^\infty \left(\frac{1}{(\gamma+\alpha)}e^{-\frac{\gamma}{w}} + \frac{w}{(\gamma+\alpha)^2}(-e^{-\frac{\gamma}{w}} + 2)\right)\mathcal{G}(w \mid \alpha, 1)\, dw$$
$$+ \int_0^\infty \left(-\frac{(-\alpha+w)}{\gamma(\gamma+\alpha)}e^{-\frac{\gamma}{w}} - \frac{(-\alpha+w)}{(\gamma+\alpha)^2}\Gamma\left(0, \frac{\gamma}{w}\right)\right)\mathcal{G}(w \mid \alpha, 1)\, dw$$
$$= \frac{1}{\alpha}\int_0^\infty \left(\frac{1}{(x+1)}e^{-\frac{x}{w'}} + \frac{w'}{(x+1)^2}(-e^{-\frac{x}{w'}} + 2)\right)\mathcal{G}\left(w' \mid \alpha, \frac{1}{\alpha}\right) dw'$$
$$+ \frac{1}{\alpha}\int_0^\infty \left(-\frac{(-1+w')}{x(x+1)}e^{-\frac{x}{w'}} - \frac{(-1+w')}{(x+1)^2}\Gamma\left(0, \frac{x}{w'}\right)\right)\mathcal{G}\left(w' \mid \alpha, \frac{1}{\alpha}\right) dw'.$$
(D.5)

Hence, $\frac{\partial}{\partial\gamma}X_{\mathrm{HK}}(x\alpha, \alpha) \sim \frac{1}{\alpha}(\frac{1}{(x+1)}e^{-x} + \frac{1}{(x+1)^2}(-e^{-x} + 2)) \sim \frac{O(1)}{\alpha}$ for large values of α. Also, the partial derivative of X with respect to α is given by

(D.6)
$$\frac{\partial}{\partial\alpha}X_{\mathrm{HK}}(x\alpha, \alpha)$$
$$= \int_0^\infty \left(\frac{w}{(\gamma+\alpha)}(-e^{-\frac{\gamma}{w}} + 2) + \frac{\Gamma(0, \frac{\gamma}{w})}{(\gamma+\alpha)}(-\alpha+w)\right)\left(\log w - \psi(\alpha)\right)\mathcal{G}(w \mid \alpha, 1)\, dw$$
$$+ \int_0^\infty \left(-\frac{w}{(\gamma+\alpha)^2}(-e^{-\frac{\gamma}{w}} + 2) - \frac{\Gamma(0, \frac{\gamma}{w})}{(\gamma+\alpha)^2}(\gamma+w)\right)\mathcal{G}(w \mid \alpha, 1)\, dw$$

$$= \int_0^\infty \left(\frac{w'}{(x+1)} \big(-e^{-\frac{x}{w'}} + 2\big) + \frac{\Gamma(0, \frac{x}{w'})}{(x+1)} \big(-1 + w'\big) \right) \big(\log w' + \log \alpha - \psi(\alpha)\big) \mathcal{G}(w' \mid \alpha, 1/\alpha)\, dw'$$
$$+ \frac{1}{\alpha} \int_0^\infty \left(- \frac{w'}{(x+1)^2} \big(-e^{-\frac{x}{w'}} + 2\big) - \frac{\Gamma(0, \frac{x}{w'})}{(x+1)^2} (x + w') \right) \mathcal{G}(w' \mid \alpha, 1/\alpha)\, dw'.$$

So, $\frac{\partial}{\partial \alpha} X_{\mathrm{HK}}(x\alpha, \alpha) = O(1) + (\frac{1}{(x+1)}(-e^{-x}+2))(\log \alpha - \psi(\alpha)) + \frac{O(1)}{\alpha} = O(1) + O(1)(\log \alpha - \psi(\alpha))$ for large values of α.

Finally, since $\lim_{\alpha \to \infty} \big(\log \alpha - \psi(\alpha)\big)/\alpha = 0$, the claim follows. ■

Appendix E. Implementation issues. Using standard identities of the Euler gamma function and permuting the terms, one rewrites (3.4) as

$$\begin{aligned} \text{(E.1)} \qquad X_{\mathrm{HK}}(\gamma, \alpha) &= \frac{(1+2\alpha)}{(\gamma+\alpha)} - \frac{2\gamma^{\alpha/2+1/2}}{(\gamma+\alpha)\Gamma(\alpha)} K_{\alpha+1}\big(2\sqrt{\gamma}\big) \\ &+ \frac{\gamma}{(\gamma+\alpha)} \\ &\times \Bigg\{ {}_2F_3(1,1;2,2,1-\alpha;\gamma) - \frac{\pi}{\sin(\pi\alpha)} \frac{\gamma^{\alpha-1}\, {}_1F_2(\alpha; 1+\alpha, 1+\alpha; \gamma)}{\Gamma(\alpha)\Gamma(1+\alpha)} \\ &+ \frac{\pi}{\sin(\pi(\alpha+1))} \frac{\gamma^{\alpha}\, {}_1F_2(1+\alpha; 2+\alpha, 2+\alpha; \gamma)}{\Gamma(\alpha)\Gamma(2+\alpha)(1+\alpha)} - \frac{\alpha}{(\alpha-1)}\, {}_2F_3(1,1;2,2,2-\alpha;\gamma) \Bigg\}, \end{aligned}$$

which is valid for $\alpha > 1$. If $\alpha < 1$, the last term $-\frac{\alpha}{(\alpha-1)}\, {}_2F_3(1,1;2,2,2-\alpha;\gamma)$ is replaced by $\frac{\pi}{\sin \pi(1-\alpha)} \frac{\alpha}{\Gamma(\alpha)\Gamma(2-\alpha)}\, {}_2F_3(1,1;2,2,2-\alpha;\gamma)$.

Either expression can be computed directly for $\alpha > 0$ if α is not an integer. When α is a positive integer, the four terms of lines three and four of (E.1) tend to $\pm\infty$. Nevertheless, it can be shown that the corresponding sum has a finite value. In the implementation used in the reported tests, we chose the simplest solution that consists in approximating $X_{\mathrm{HK}}(\gamma, \alpha)$ by interpolation of the values $X_{\mathrm{HK}}(\gamma, n - 10^{-7})$ and $X_{\mathrm{HK}}(\gamma, n + 10^{-7})$ in the interval $n - 10^{-7} \le \alpha \le n + 10^{-7}$, where n is an integer. On the other hand, the first two terms of (E.1) are well-defined for any value of $\alpha > 0$.

Similar remarks apply to the computation of U_{HK}. In particular, one obtains

$$\begin{aligned} \text{(E.2)} \qquad U_{\mathrm{HK}}(\gamma, \alpha) &= -\gamma_E - \log(\gamma+\alpha) + \psi(\alpha) \\ &+ \frac{\pi}{\sin(\pi\alpha)} \frac{\gamma^{\alpha}\, {}_1F_2(\alpha; 1+\alpha, 1+\alpha; \gamma)}{\alpha\Gamma(\alpha)\Gamma(\alpha+1)} + \frac{\gamma}{(\alpha-1)}\, {}_2F_3(1,1;2,2,2-\alpha;\gamma), \end{aligned}$$

which is valid for $\alpha > 1$. If $\alpha < 1$, the last term $\frac{\gamma}{(\alpha-1)}\, {}_2F_3(1,1;2,2,2-\alpha;\gamma)$ is replaced by $-\frac{\pi}{\sin \pi(1-\alpha)} \frac{\gamma}{\Gamma(\alpha)\Gamma(2-\alpha)}\, {}_2F_3(1,1;2,2,2-\alpha;\gamma)$. These expressions are valid for α not an integer. One uses an approximation as explained above for values of α near integers.

Appendix F. Method in [8] revisited. The method in [8] is equivalent to solving the following (nonlinear) system of equations in the variables ε^2, σ^2, and α:

$$\begin{aligned} \text{(F.1)} \qquad & E[I] = \overline{I}, \\ & E[I^2]/E[I]^2 = \overline{I^2}/\overline{I}^2 := M, \\ & E[I^3]/E[I]^3 = \overline{I^3}/\overline{I}^3 := L. \end{aligned}$$

Sufficient and necessary conditions for this system to admit a solution are presented below. For that purpose, the change of variables (3.2) was adopted.

Proposition F.1. *Let $A = \sqrt{I}$ be distributed according to the homodyned K-distribution $P_{\mathrm{HK}}(A \mid \varepsilon, \sigma^2, \alpha)$. With the notation of (3.2), one has*

$$E[I^2]/E[I]^2 = M_{\mathrm{HK}}(\gamma, \alpha) = \frac{(\gamma^2 + 4\gamma\alpha + 2\alpha(\alpha+1))}{(\gamma+\alpha)^2}, \tag{F.2}$$

$$E[I^3]/E[I]^3 = L_{\mathrm{HK}}(\gamma, \alpha) = \frac{(\gamma^3 + 9\gamma^2\alpha + 18\gamma\alpha(\alpha+1) + 6\alpha(\alpha+1)(\alpha+2))}{(\gamma+\alpha)^3}. \tag{F.3}$$

As one can see, (F.2) and (F.3) depend only on the variables γ and α. Thus, the method in [8] amounts to solving (F.2) and (F.3) in the variables γ and α and then using (3.5) with $\mu = E[I]$.

Let $\alpha > 0$ be known. Using (F.2), one deduces the value of $\gamma \geq 0$ explicitly.

Proposition F.2. *Let $M > 1$ be a real number and α be fixed. Then, there exists at most one solution $\gamma \geq 0$ to the equation $M_{\mathrm{HK}}(\gamma, \alpha) = M$, namely*

$$\gamma = \Big(\alpha(2-M) + \sqrt{2(M-1)\alpha + (2-M)\alpha^2}\Big)\big/(M-1). \tag{F.4}$$

(a) *If $M \leq 2$, then there is a solution for any $\alpha > 0$.*

(b) *If $M > 2$, then there is a solution if and only if $0 < \alpha \leq \alpha_0 = M_{\mathrm{K}}^{-1}(M) = 2/(M-2)$.*

Thus, one obtains a well-defined function $\gamma = \gamma(\alpha, M)$ on the domain described by Proposition F.2. Next, proceeding as in section 3.3, the expression of (F.4) is substituted in (F.3), thus yielding a function $L_{\mathrm{HK}}(\gamma(\alpha, M), \alpha)$ in the single variable α.

Proposition F.3. *Let $M > 1$ be a real number.*

(a) *One has the left boundary condition $\lim_{\alpha\to 0} L_{\mathrm{HK}}(\gamma(\alpha, M), \alpha) = \infty$.*

(b) *If $M \leq 2$, then $\lim_{\alpha\to\infty} L_{\mathrm{HK}}(\gamma(\alpha, M), \alpha) = L_{\mathrm{Ri}}(\kappa_0)$, where $\kappa_0 = M_{\mathrm{Ri}}^{-1}(M) = 1/(1-\sqrt{2-M}) - 1$.*

(c) *If $M > 2$, then $\lim_{\alpha\to\alpha_0} L_{\mathrm{HK}}(\gamma(\alpha, M), \alpha) = L_{\mathrm{K}}(\alpha_0)$, where $\alpha_0 = M_{\mathrm{K}}^{-1}(M) = 2/(M-2)$.*

(d) *The function $L_{\mathrm{HK}}(\gamma(\alpha, M), \alpha)$ is decreasing on its domain.*

In Proposition F.3(b), the functions $M_{\mathrm{K}}(\alpha) = 2\big(1+1/\alpha\big)$ and $L_{\mathrm{K}}(\alpha) = 6\big(1+1/\alpha\big)\big(1+2/\alpha\big)$ correspond to the computation of the M- and L-statistics for the K-distribution. In part (c), the functions $M_{\mathrm{Ri}}(\kappa) = 2 - \frac{\kappa^2}{(\kappa+1)^2}$ and $L_{\mathrm{Ri}}(\kappa) = \frac{(\kappa^3+9\kappa^2+18\kappa+6)}{(\kappa+1)^3}$ correspond to the computation of the M- and L-statistics for the Rice distribution.

Part (d) of the proposition implies that a binary search algorithm can be used to find the unique solution to (F.2) and (F.3), whenever a solution exists.

Corollary F.4. *Let $M > 1$ and $L > 1$ be given. Then, there exists a simultaneous solution to the system $M_{\mathrm{HK}}(\gamma, \alpha) = M$ and $L_{\mathrm{HK}}(\gamma, \alpha) = L$ if and only if*

(a) *$M \leq 2$ and $L > L_{\mathrm{Ri}}(M_{\mathrm{Ri}}^{-1}(M))$, or*

(b) *$M > 2$ and $L > L_{\mathrm{K}}(M_{\mathrm{K}}^{-1}(M))$.*

Moreover, if a solution exists, it is unique.

Thus, one obtains well-defined functions $\gamma = \gamma(M, L)$ and $\alpha = \alpha(M, L)$, where M and L are restricted to the domain described by parts (a) and (b) of Corollary F.4.

Acknowledgments. We thank Mr. D. P. Hruska and Prof. M. L. Oelze for letting us use their MATLAB implementation of their method [11] in the reported tests. We also thank the anonymous reviewers for their helpful comments on the presentation of this work.

REFERENCES

[1] D. A. Abraham and A. P. Lyons, *Novel physical interpretation of K-distributed reverberation*, IEEE J. of Ocean. Eng., 27 (2002), pp. 800–813.

[2] M. Abramowitz and I. A. Stegun, eds., *Handbook of Mathematical Functions with Formulas, Graphs, and Mathematical Tables*, Dover, New York, 1972.

[3] M. Alavi, F. Destrempes, C. Schmitt, E. Montagnon, and G. Cloutier, *Shear wave propagation modulates quantitative ultrasound K-distribution echo envelope model statistics in homogeneous viscoelastic phantoms*, in Proceedings of the IEEE International Ultrasonics Symposium, Dresden, Germany, 2012.

[4] D. Blacknell and R. J. A. Tough, *Parameter estimation for the K-distribution based on* $[z \log(z)]$, IEE Proc. Radar, Sonar Navig., 148 (2001), pp. 309–312.

[5] C. B. Burckhardt, *Speckle in ultrasound B-mode scans*, IEEE Trans. Sonics Ultrason., SU-25 (1978), pp. 1–6.

[6] F. Destrempes and G. Cloutier, *A critical review and uniformized representation of statistical distributions modeling the ultrasound echo envelope*, Ultrasound Med. Biol., 36 (2010), pp. 1037–1051.

[7] F. Destrempes, E. Franceschini, F. T. H. Yu, and G. Cloutier, *Relation between the backscatter coefficient and echo envelope statistical parameters in the context of red blood cell aggregation*, in Proceedings of the 8th International Conference on Ultrasonic Biomedical Microscanning, St-Paulin, QC, Canada, 2012.

[8] V. Dutt and J. F. Greenleaf, *Ultrasound echo envelope analysis using a homodyned K distribution signal model*, Ultrason. Imaging, 16 (1994), pp. 265–287.

[9] C. F. Gerald and P. O. Wheatley, eds., *Applied Numerical Analysis*, 7th ed., Addison-Wesley, Reading, MA, 2003.

[10] X. Hao, C. J. Bruce, C. Pislaru, and J. F. Greenleaf, *Characterization of reperfused infarcted myocardium from high-frequency intracardiac ultrasound imaging using homodyned K distribution*, IEEE Trans. Ultrason. Ferroelectr. Freq. Control., 49 (2002), pp. 1530–1542.

[11] D. P. Hruska and M. L. Oelze, *Improved parameter estimates based on the homodyned K distribution*, IEEE Trans. Ultrason. Ferroelectr. Freq. Control, 56 (2009), pp. 2471–2481.

[12] D. P. Hruska, J. Sanchez, and M. L. Oelze, *Improved diagnostics through quantitative ultrasound imaging*, in Proceedings of the Annual International Conference of the IEEE Engineering in Medicine and Biology Society, 2009, pp. 1956–1959.

[13] E. Jakeman, *On the statistics of K-distributed noise*, J. Phys. A, 13 (1980), pp. 31–48.

[14] E. Jakeman and P. N. Pusey, *A model for non-Rayleigh sea echo*, IEEE Trans. Antennas and Propagation, 24 (1976), pp. 806–814.

[15] E. Jakeman and R. J. A. Tough, *Generalized K distribution: A statistical model for weak scattering*, J. Opt. Soc. Am. A, 4 (1987), pp. 1764–1772.

[16] J. Jensen, *Sur les fonctions convexes et les inégalités entre les valeurs moyennes*, Acta Math., 30 (1906), pp. 175–193.

[17] J. A. Jensen, *A program for simulating ultrasound systems*, Med. Biol. Comput., 34 (1996), pp. 351–353.

[18] J. A. Jensen and N. B. Svendsen, *Calculation of pressure fields from arbitrarily shaped, apodized, and excited ultrasound transducers*, IEEE Trans. Ultrason. Ferroelectr. Freq. Control, 39 (1992), pp. 262–267.

[19] F. Kallel, M. Bertrand, and J. Meunier, *Speckle motion artifact under tissue rotation*, IEEE Trans. Ultrason. Ferroelectr. Freq. Control, 41 (1994), pp. 105–122.

[20] S. Kullback and R. A. Leibler, *On information and sufficiency*, Ann. Math. Statistics, 22 (1951), pp. 79–86.

[21] R. D. Lord, *The use of the Hankel transform in statistics.* I. *General theory and examples*, Biometrika, 41 (1954), pp. 44–55.

[22] J. Mamou, A. Coron, M. L. Oelze, E. Saegusa-Beecroft, M. Hata, P. Lee, J. Machi, E. Yanagihara, P. Laugier, and E. J. Feleppa, *Three-dimensional high-frequency backscatter and envelope quantification of cancerous human lymph nodes*, Ultrasound Med. Biol., 37 (2011), pp. 2055–2068.

[23] R. C. Molthen, P. M. Shankar, and J. M. Reid, *Characterization of ultrasonic B-scans using non-Rayleigh statistics*, Ultrasound Med. Biol., 21 (1995), pp. 161–170.

[24] M. Nakagami, *Study of the resultant amplitude of many vibrations whose phases and amplitudes are at random*, J. Inst. Elec. Commun. Engrs. Japan, 24 (1940), pp. 17–26.

[25] M. L. Oelze and W. D. O'Brien, Jr., *Quantitative ultrasound assessment of breast cancer using a multiparameter approach*, in Proceedings of the IEEE Utrasound Symposium, 2007, pp. 981–984.

[26] C. J. Oliver, *A model for non-Rayleigh scattering statistics*, in Wave Propagation and Scattering, B. J. Uscinski, ed., Clarendon, Oxford, UK, 1986, pp. 155–173.

[27] G. Parry and P. N. Pusey, *K-distributions in atmospheric propagation of laser light*, J. Opt. Soc. Am., 69 (1979), pp. 796–798.

[28] R. W. Prager, A. H. Gee, G. M. Treece, and L. H. Berman, *Decompression and speckle detection for ultrasound images using the homodyned K-distribution*, Pattern Recogn. Lett., 24 (2003), pp. 705–713.

[29] Lord Rayleigh, *On the resultant of a large number of vibrations of the same pitch and of arbitrary phase*, Phil. Mag., 10 (1880), pp. 73–78.

[30] S. O. Rice, *Mathematical analysis of random noise*, Bell System Tech. J., 24 (1945), pp. 46–156.

[31] R. K. Saha and M. C. Kolios, *Effects of cell spatial organization and size distribution on ultrasound backscattering*, IEEE Trans. Ultrason. Ferroelectr. Freq. Control., 58 (2011), pp. 2118–2131.

[32] D. Savéry and G. Cloutier, *High-frequency ultrasound backscattering by blood: Analytical and semi-analytical models of the erythrocyte cross section*, J. Acoust. Soc. Am., 121 (2007), pp. 3963–3971.

[33] P. M. Shankar, J. M. Reid, H. Ortega, C. W. Piccoli, and B. B. Goldberg, *Use of non-Rayleigh statistics for the identification of tumors in ultrasonic B-scans of the breast*, IEEE Trans. Med. Imag., 12 (1993), pp. 687–692.

[34] R. Taggart, R. E. Baddour, A. Giles, G. J. Czarnota, and M. C. Kolios, *Ultrasonic characterization of whole cells and isolated nuclei*, Ultrasound Med. Biol., 33 (2007), pp. 389–401.

[35] I. Trop, F. Destrempes, M. El Khoury, L. Allard, B. Chayer, and G. Cloutier, *The added value of statistical parameters based on sonographic backscattering properties of tissues in the management of breast lesions*, in Proceedings of the 98th Assembly and Annual Meeting of the Radiological Society of North America, Chicago, IL, 2012.

[36] V. Twersky, *Transparency of pair-correlated, random distributions of small scatterers, with applications to the cornea*, J. Opt. Soc. Am., 65 (1975), pp. 524–530.

[37] V. Twersky, *Low-frequency scattering by correlated distributions of randomly oriented particles*, J. Acoust. Soc. Am., 81 (1987), pp. 1609–1618.

[38] K. D. Ward, *Compound representation of high resolution sea clutter*, Electron. Lett., 17 (1981), pp. 561–566.